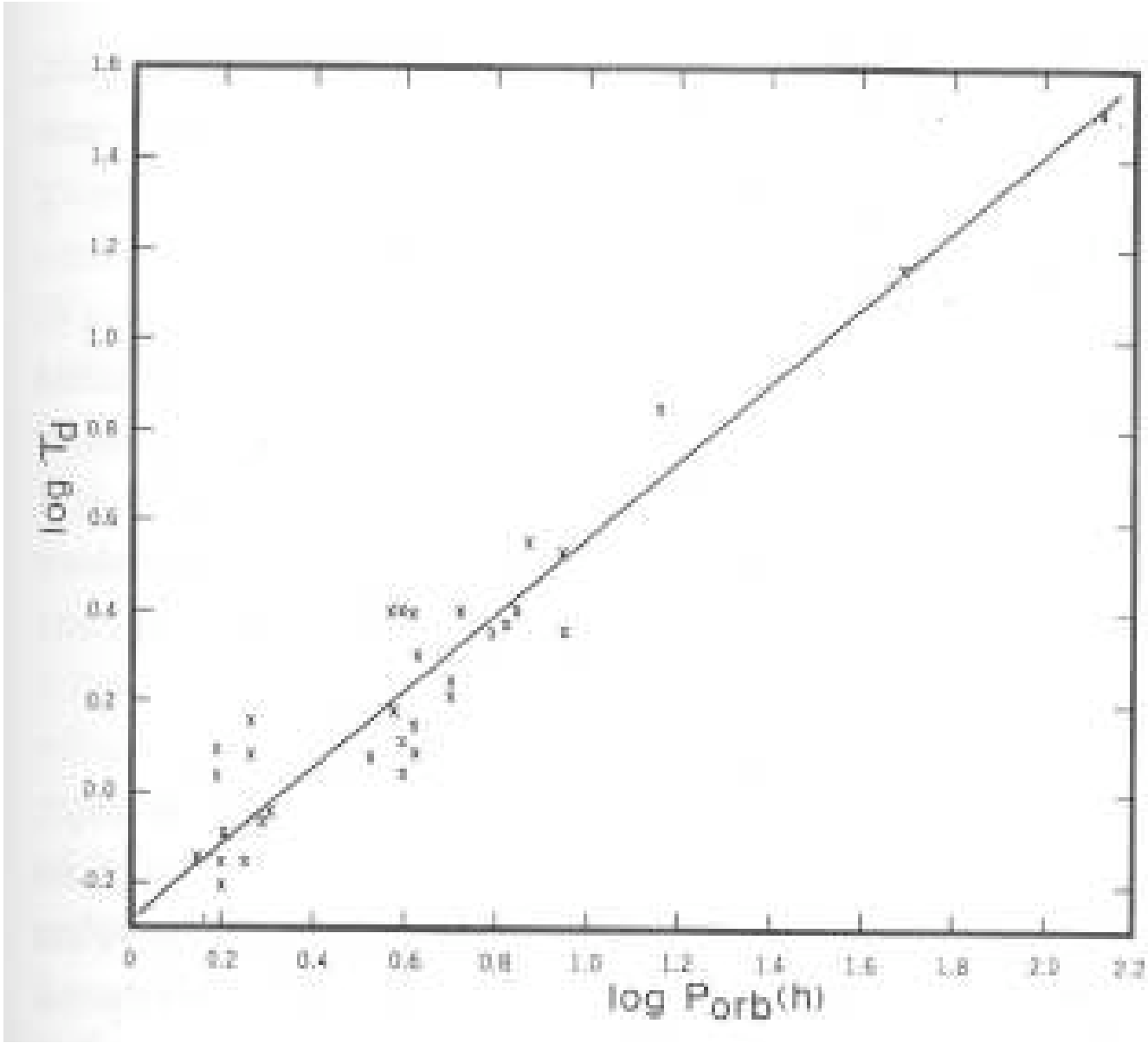
log $L_{bol}$
log $P_{orb}$(h)
1.6
1.4
1.2
1.0
0.8
0.6
0.4
0.2
0.0
-0.2
0
0.2
0.4
0.6
0.8
1.0
1.2
1.4
1.6
1.8
2.0
2.2

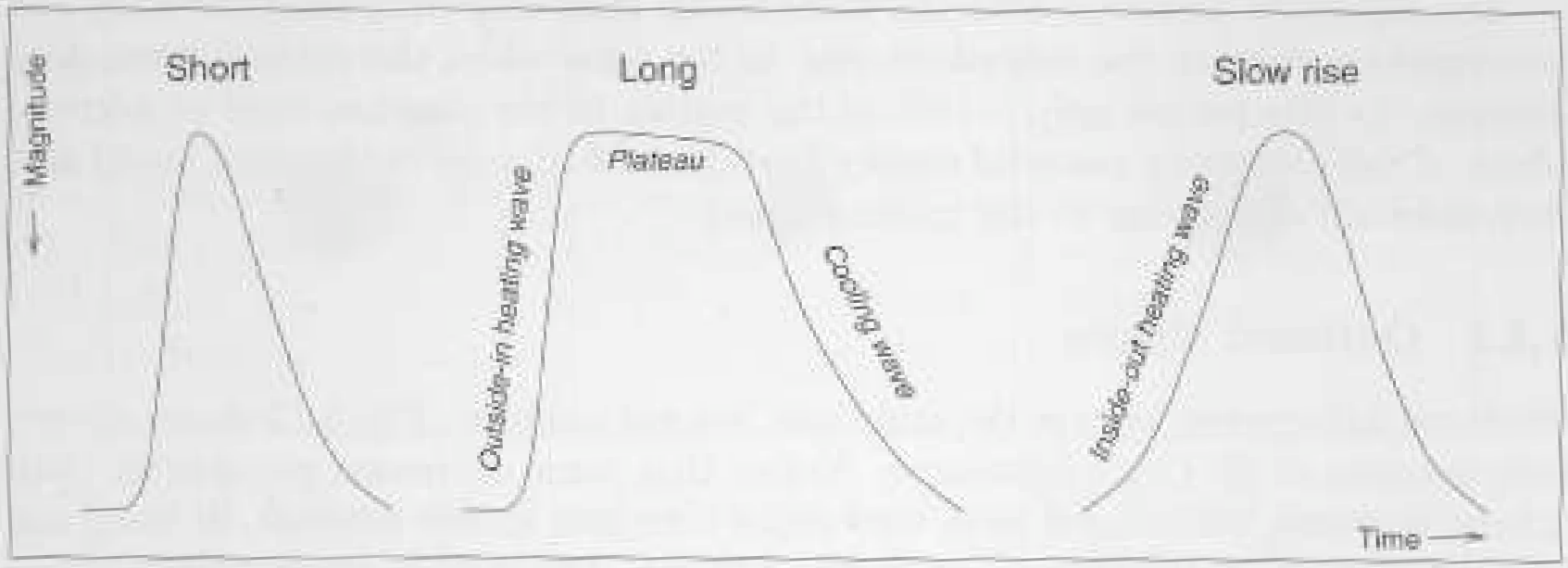


Fig. 5.13: Schematic outburst types, for comparison with the data in Fig. 5.12. The different shapes are explained in the text. Since all observed outbursts are subtly different, one could, should one wish, divide them into many more types.

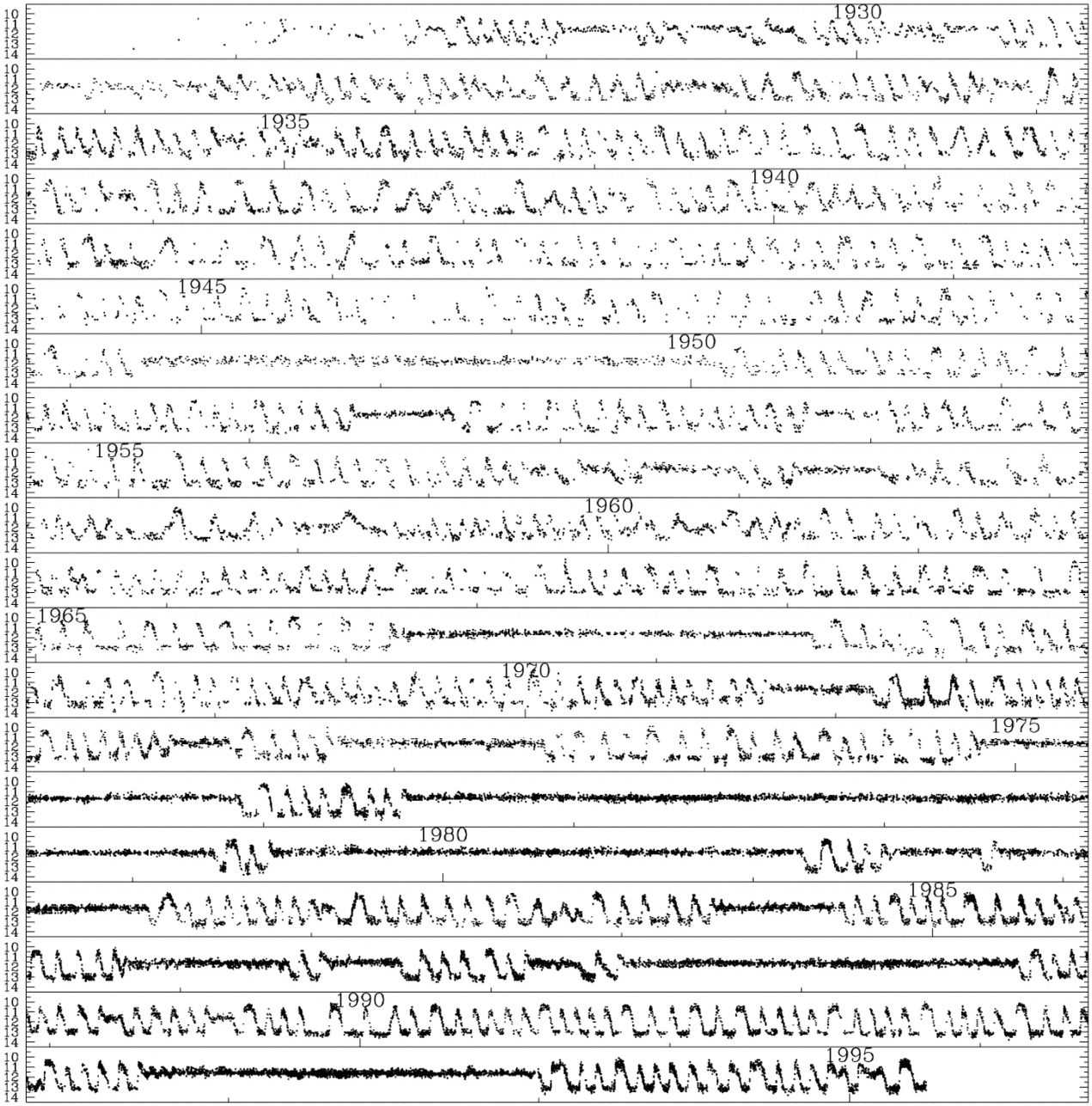
1930
1935
1940
1945
1950
1955
1960
1965
1970
1975
1980
1985
1990
1995

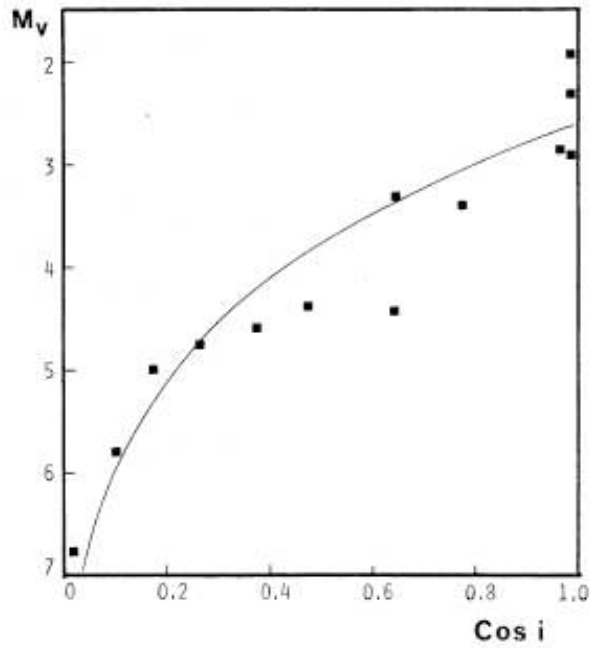


**Figure 2.** Correlation between absolute magnitude $M_V$ and orbital (or disc) inclination.

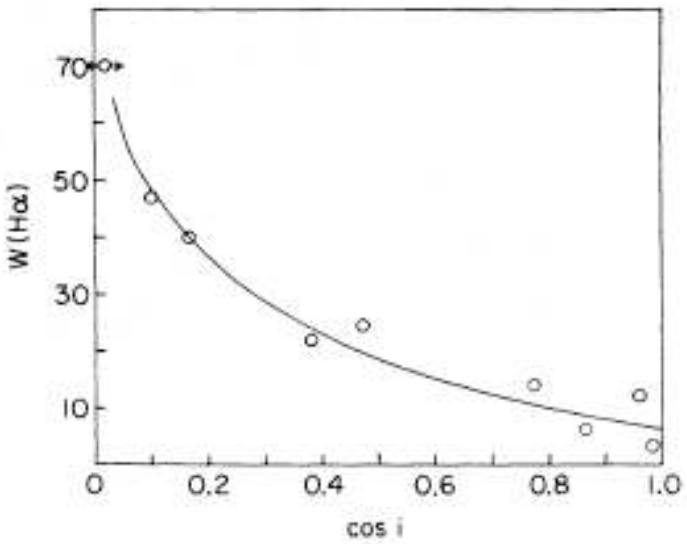


Dependence of H$\alpha$ equivalent width on orbital inclination for classical nova remnants.

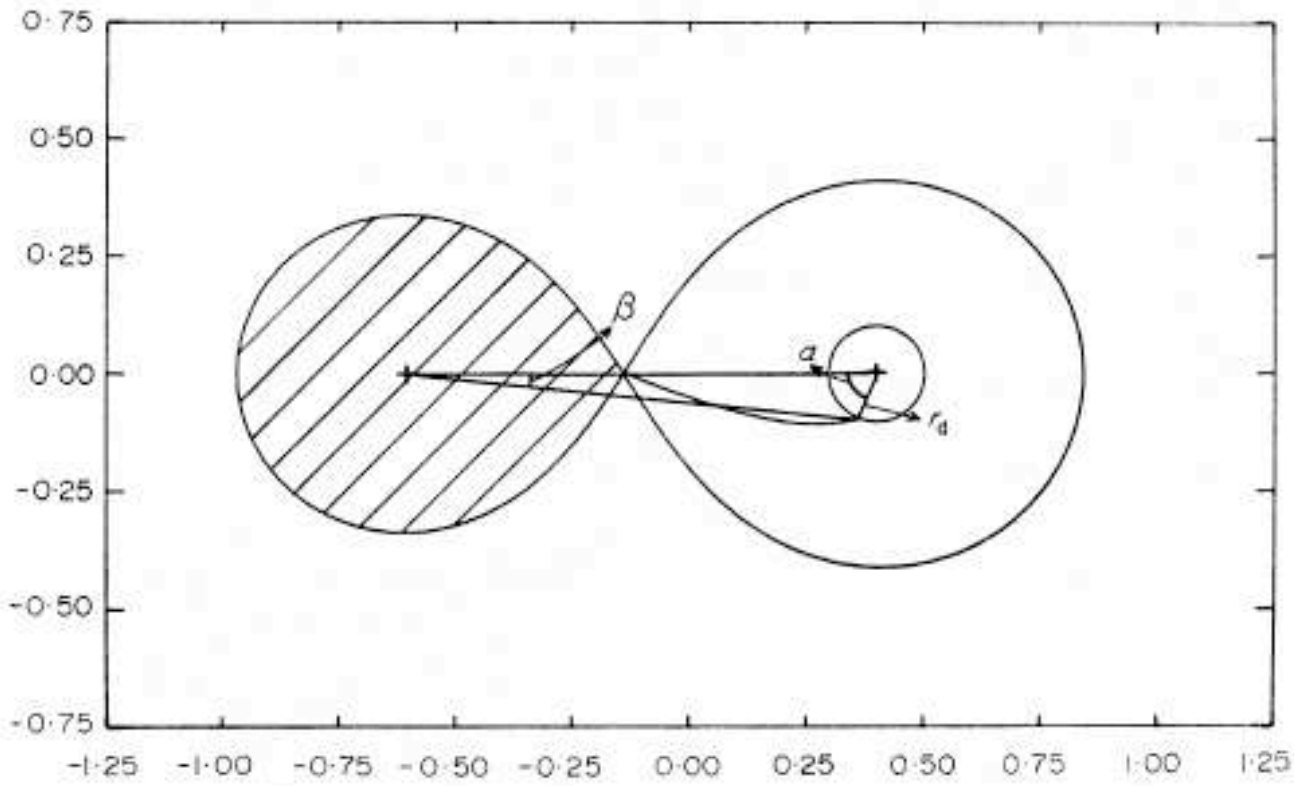


FIG. 1. *The particle trajectory hot spot model for a mass fraction of* 0·6. *The spot forms at the intersection of the trajectory from the inner Lagrangian point and the ring around the blue star at radius* $r_d$. *The bounding curve is the Roche equipotential through* $L_1$ *in the orbital plane.*

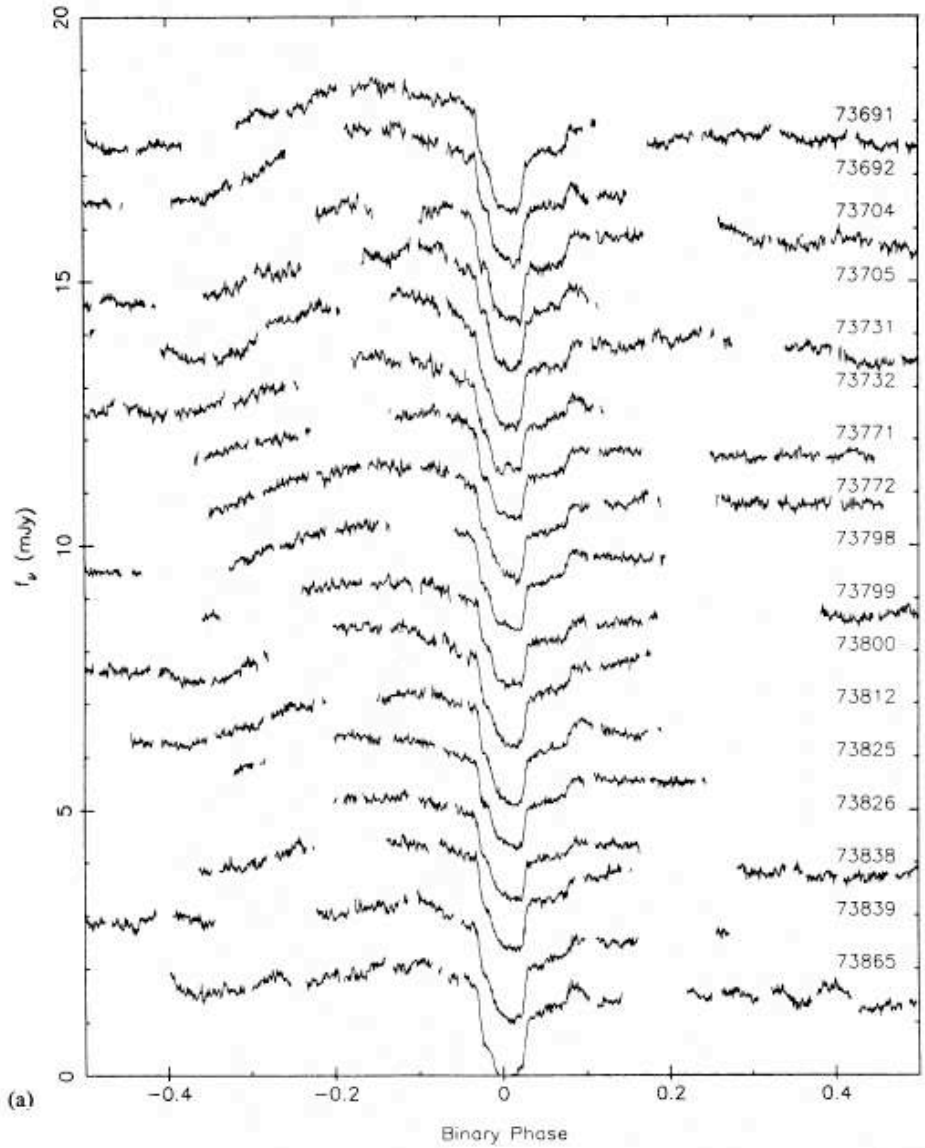


**Figure 1.** (a) Individual white light curves at 5 s time resolution (observed at CTIO). Each light curve is offset by 1 mJy from the next. The bottom light curve, cycle 73865, is at its measured flux density. (b) *U*, *R* and *B* light curves. *U* and *R* are at 10 s time resolution, *B* is at 15 s time resolution. Each light curve is offset by 3 mJy from the next, with cycle 73893 (B) at its measured flux density. (c) Individual white light curves at 5 s time resolution (observed at SAAO). Each light curve is offset by 1.5 mJy from the next. The bottom light curve, cycle 73876, is at its measured flux density.

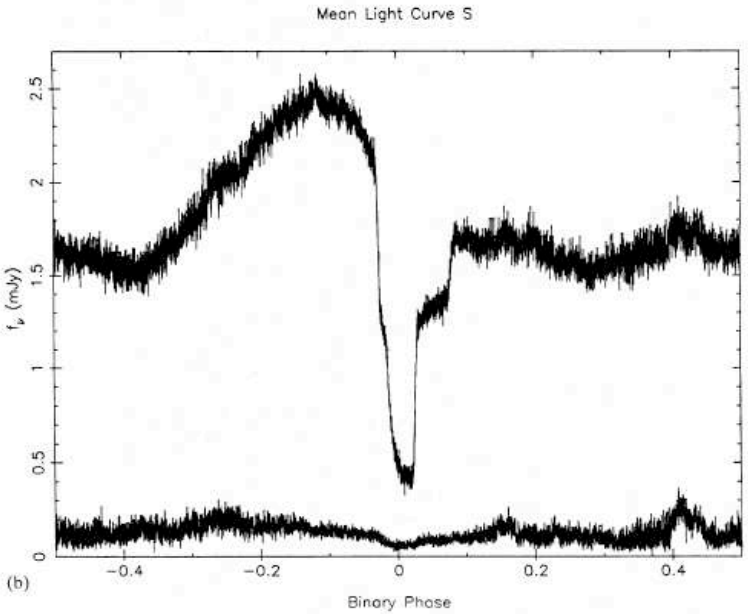


**Figure 2.** (a) Average of the 17 white light curves observed at CTIO at 1 s time resolution. The lower curve is a measure of the uncertainty in the mean light curve. (b) Average of the 12 white light curves observed at SAAO at 1 s time resolution. The lower curve is a measure of the uncertainty in the mean light curve.

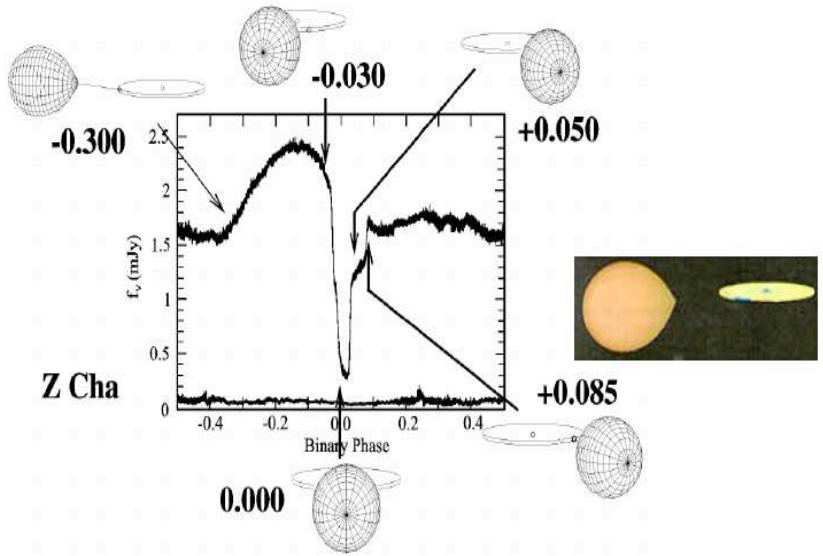

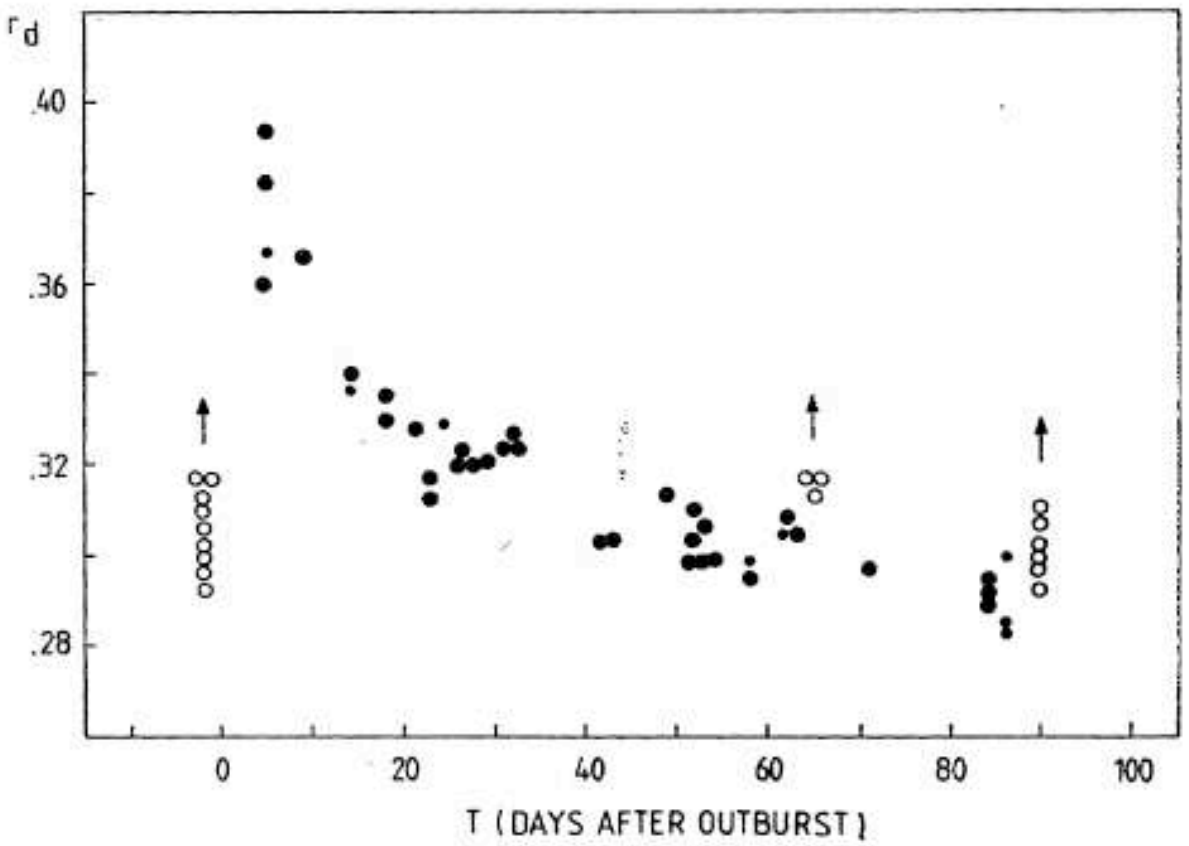


Fig. 1. Variations of the disk-radius. Small symbols are of lower weight. Open circles are from eclipses observed at the onset of an outburst.

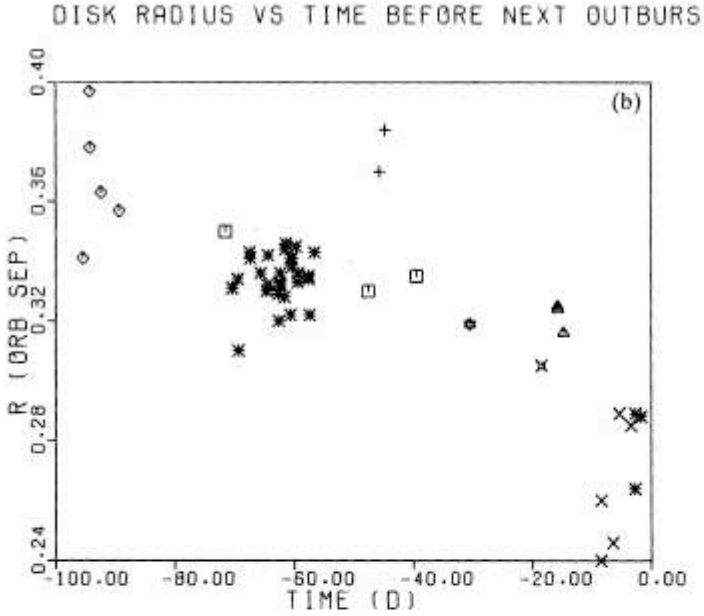


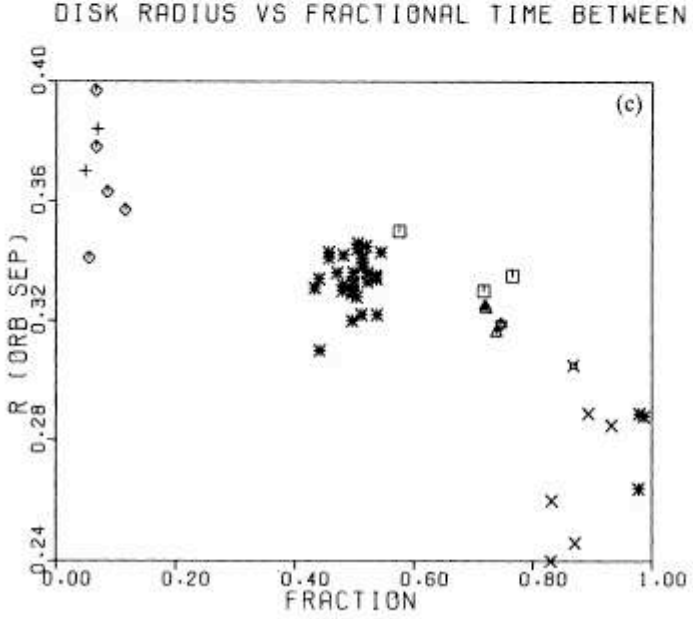


**Figure 1** – *continued*

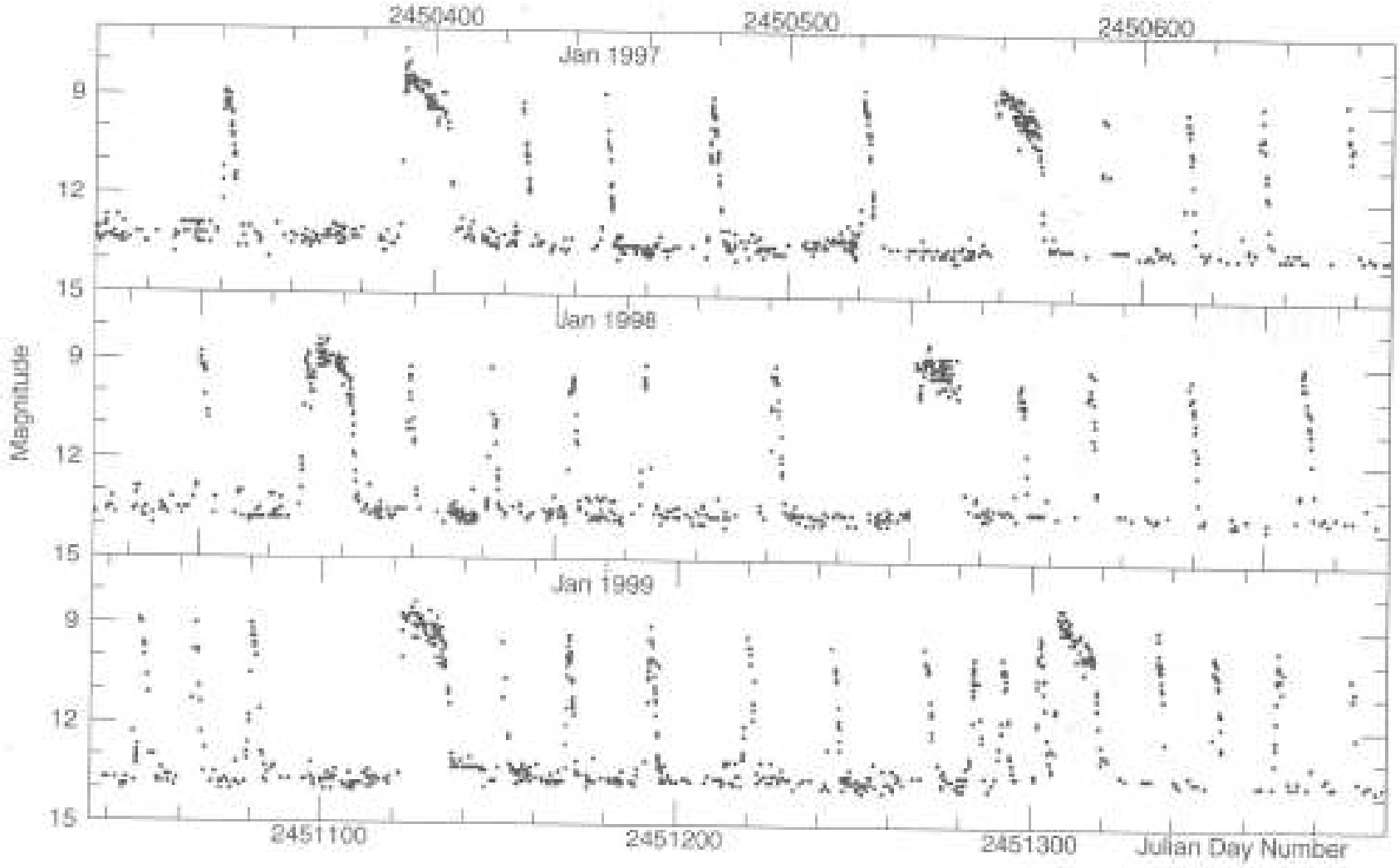


Fig. 6.1: A 3-yr section of VW Hyi's lightcurve showing both normal outbursts and superoutbursts. (Data by the Royal Astronomical Society of New Zealand.)

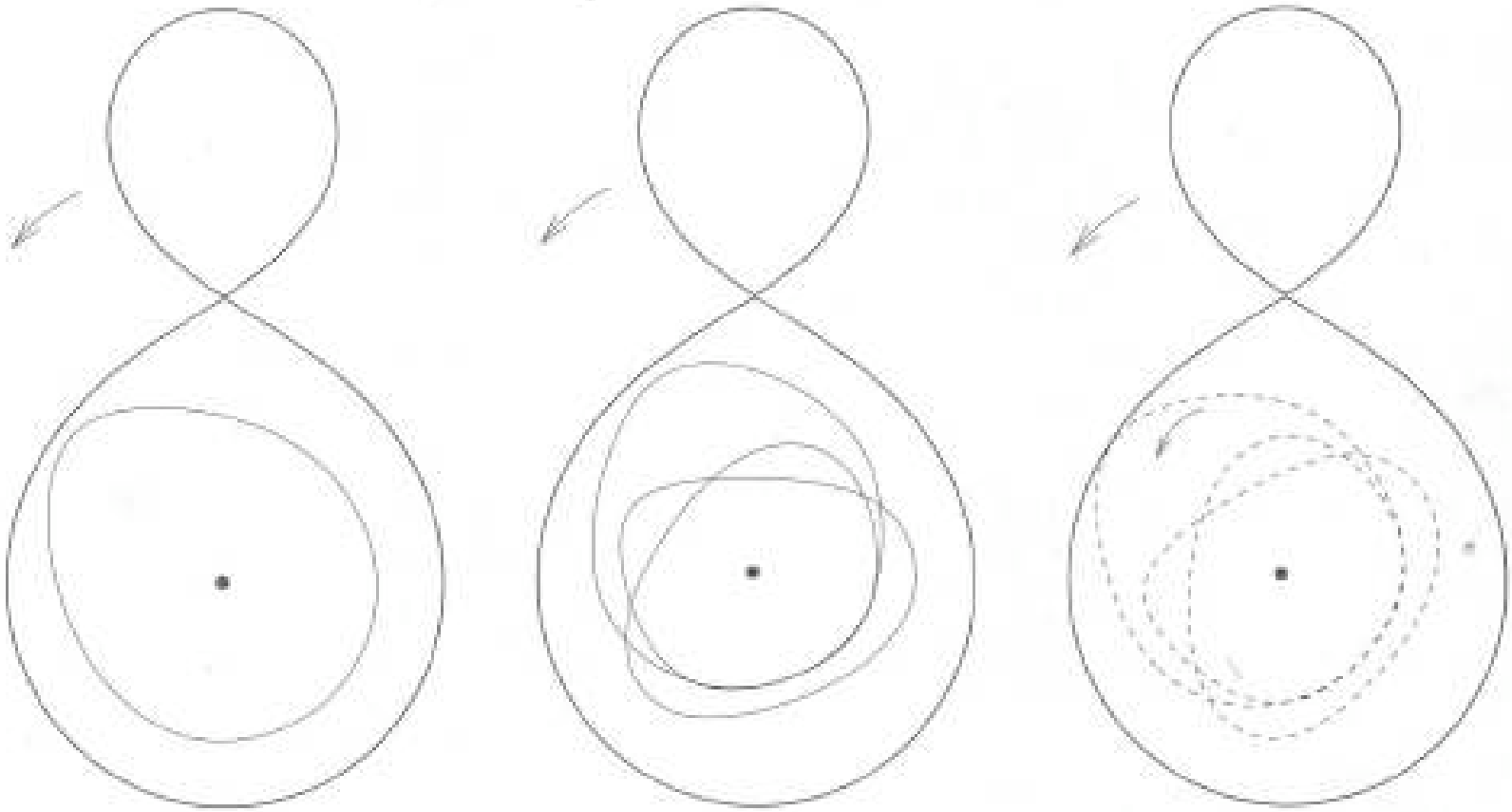

Fig. 6.4: In systems with high mass ratios the orbits in the outer disc are distorted by the presence of the secondary, and form a tidal bulge slightly ahead of the secondary (left panel). If a resonance sets in, the orbit is no longer fully periodic; a particle orbits three times in the time the secondary orbits once (middle panel) producing a three-petalled orbit. Such orbits precess slowly (right panel), so the eccentricity of the disc precesses.

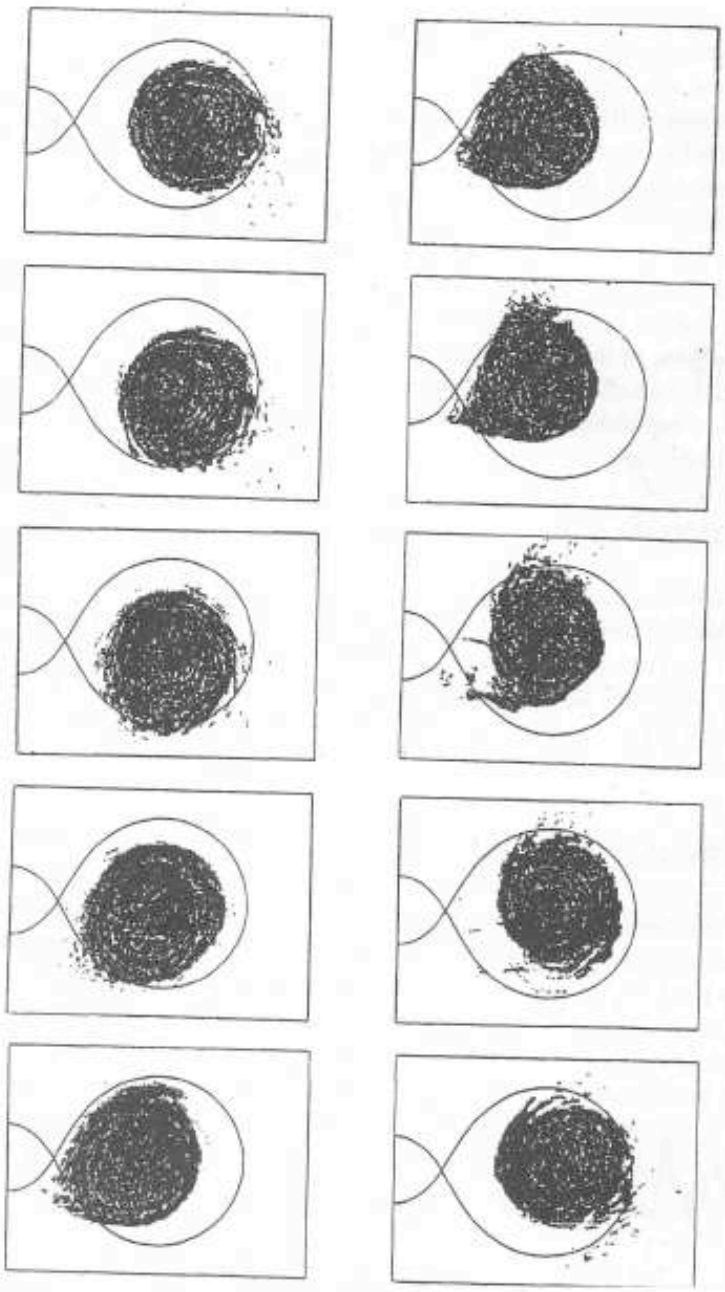

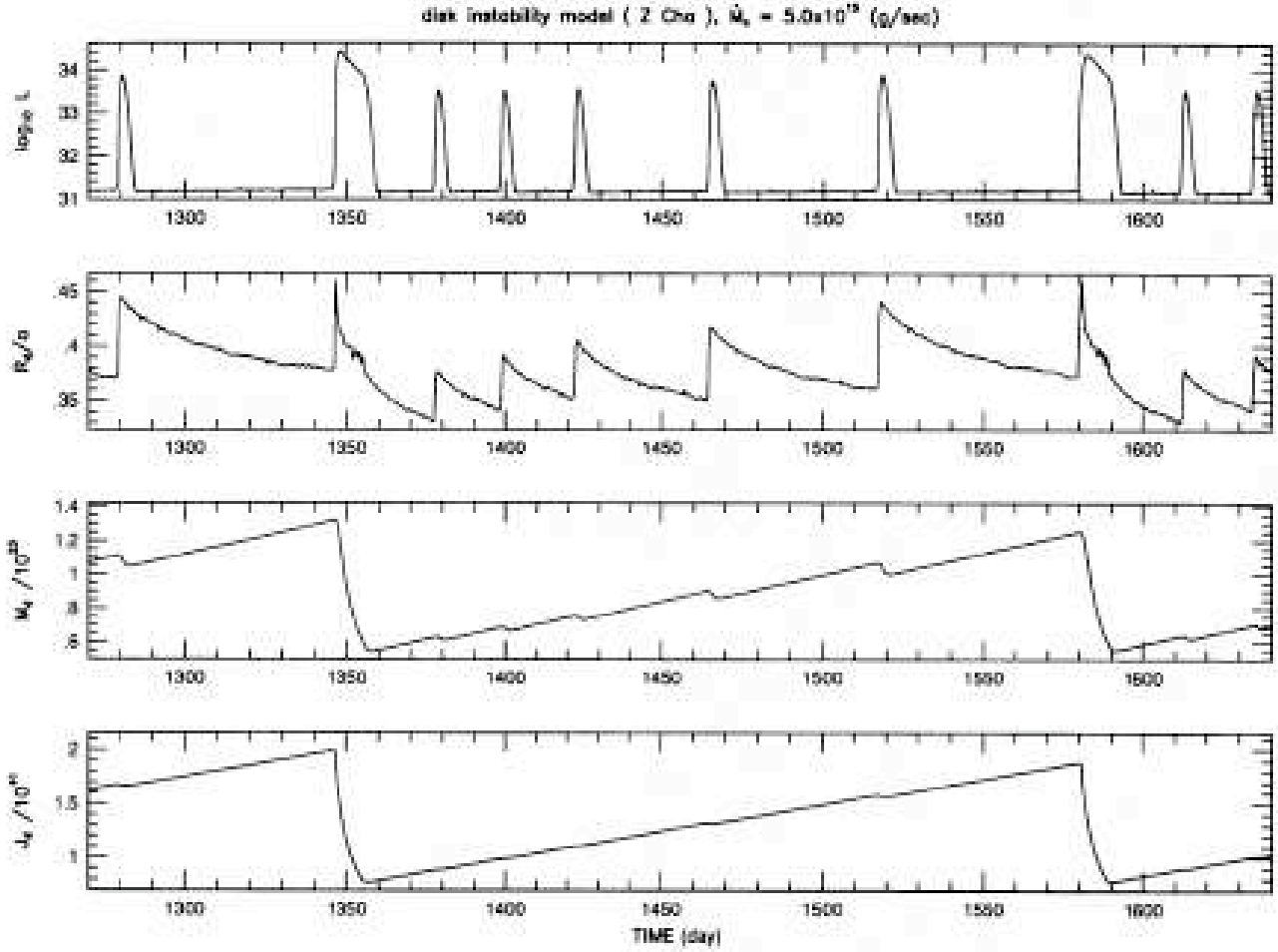


Fig. 1. Time evolution of the accretion disk for a complete superoutburst cycle based on the disk-instability model. The viscosity parameter ($\alpha$) used is that of case A. From top to bottom: (1) the bolometric luminosity of the disk, (2) the disk radius $R_{\rm d}$ in unit of the binary separation ($a$), (3) the total disk mass ($M_{\rm d}$), and (4) the total angular momentum of the disk ($J_{\rm d}$) as functions of time (in unit of days).

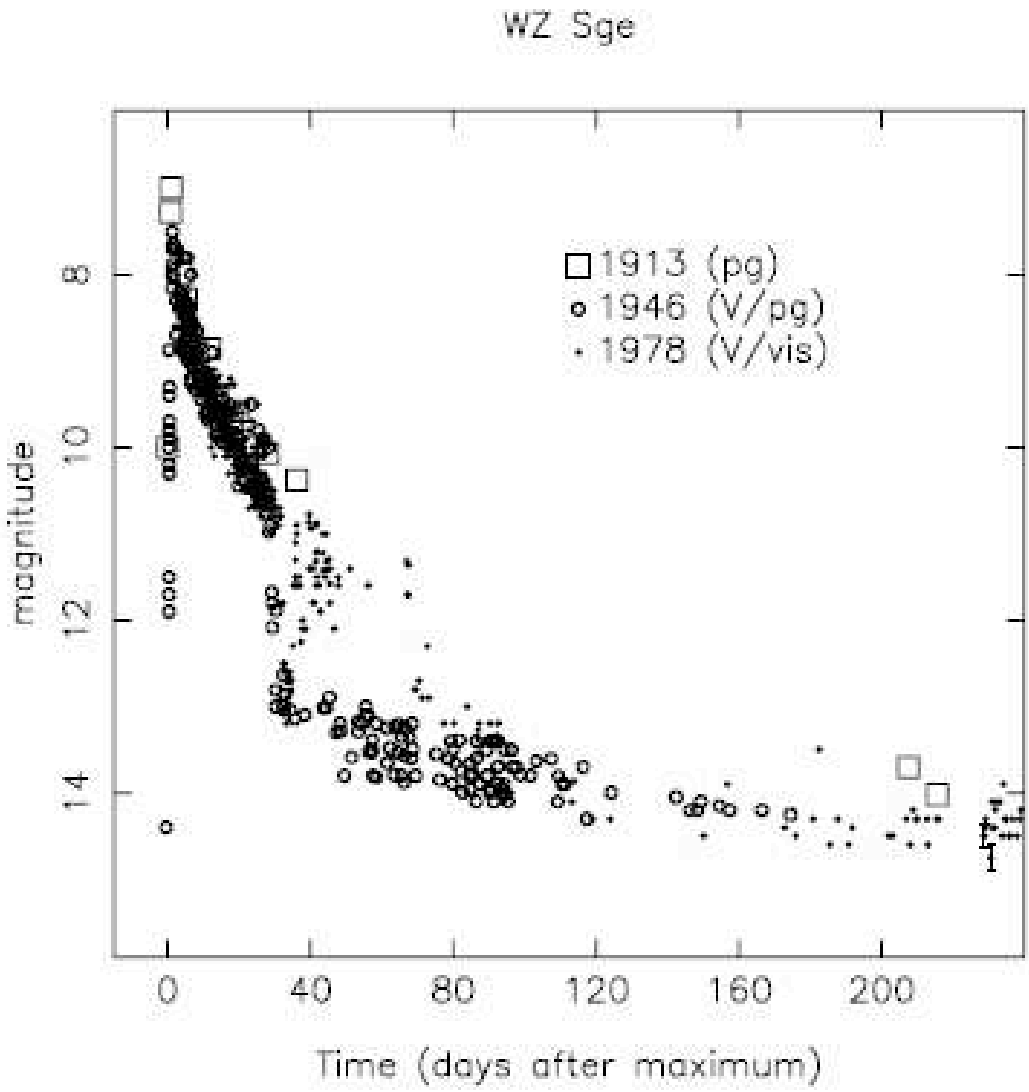


**Figure 2.** A plot of optical magnitude during the 1913, 1946 and 1978 outbursts of WZ Sge, from Kuulkers (2000). Reprinted with permission from Elsevier.

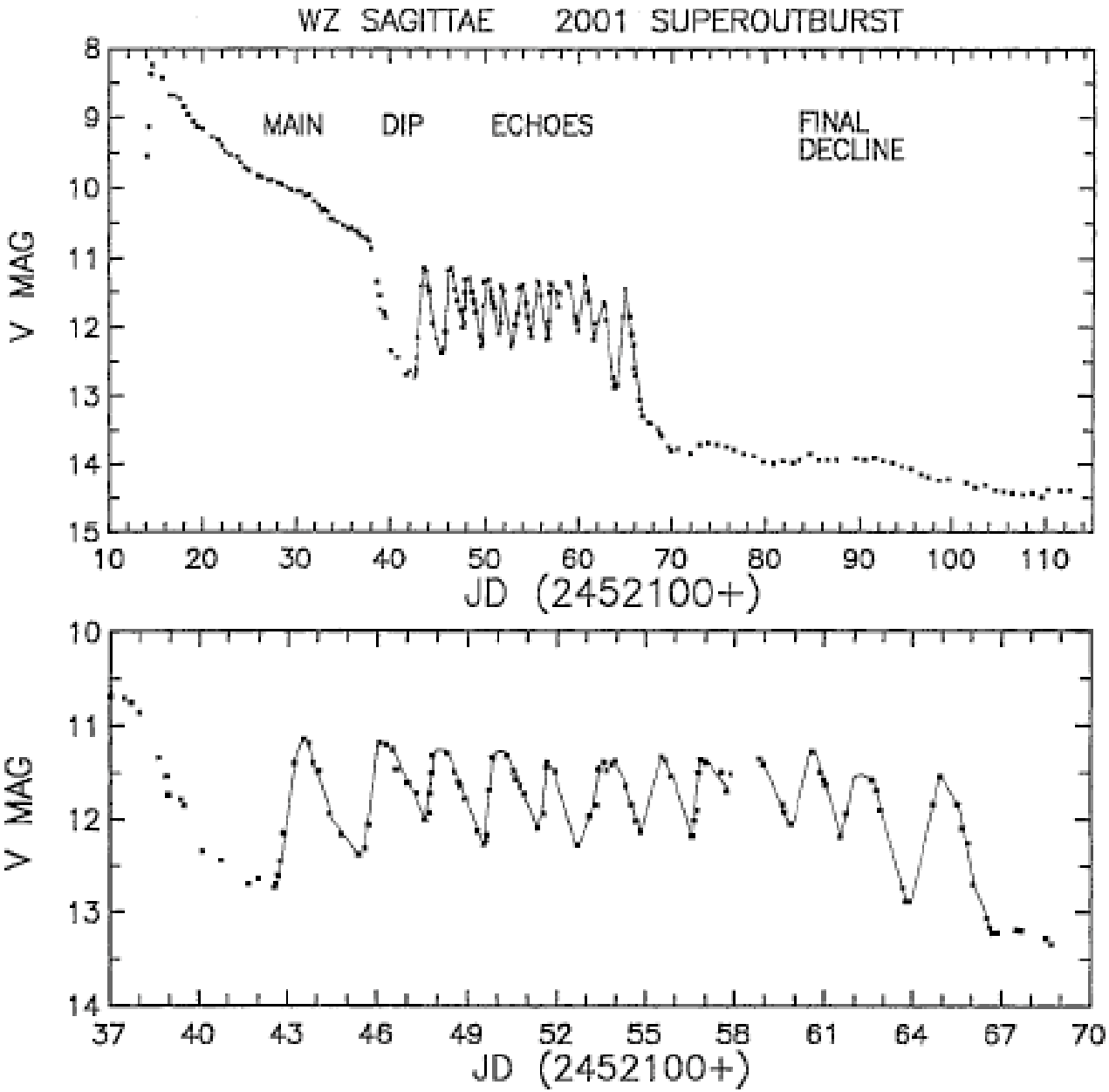
WZ SAGITTAE 2001 SUPEROUTBURST
MAIN
DIP
ECHOES
FINAL DECLINE
V MAG
JD (2452100+)
V MAG
JD (2452100+)

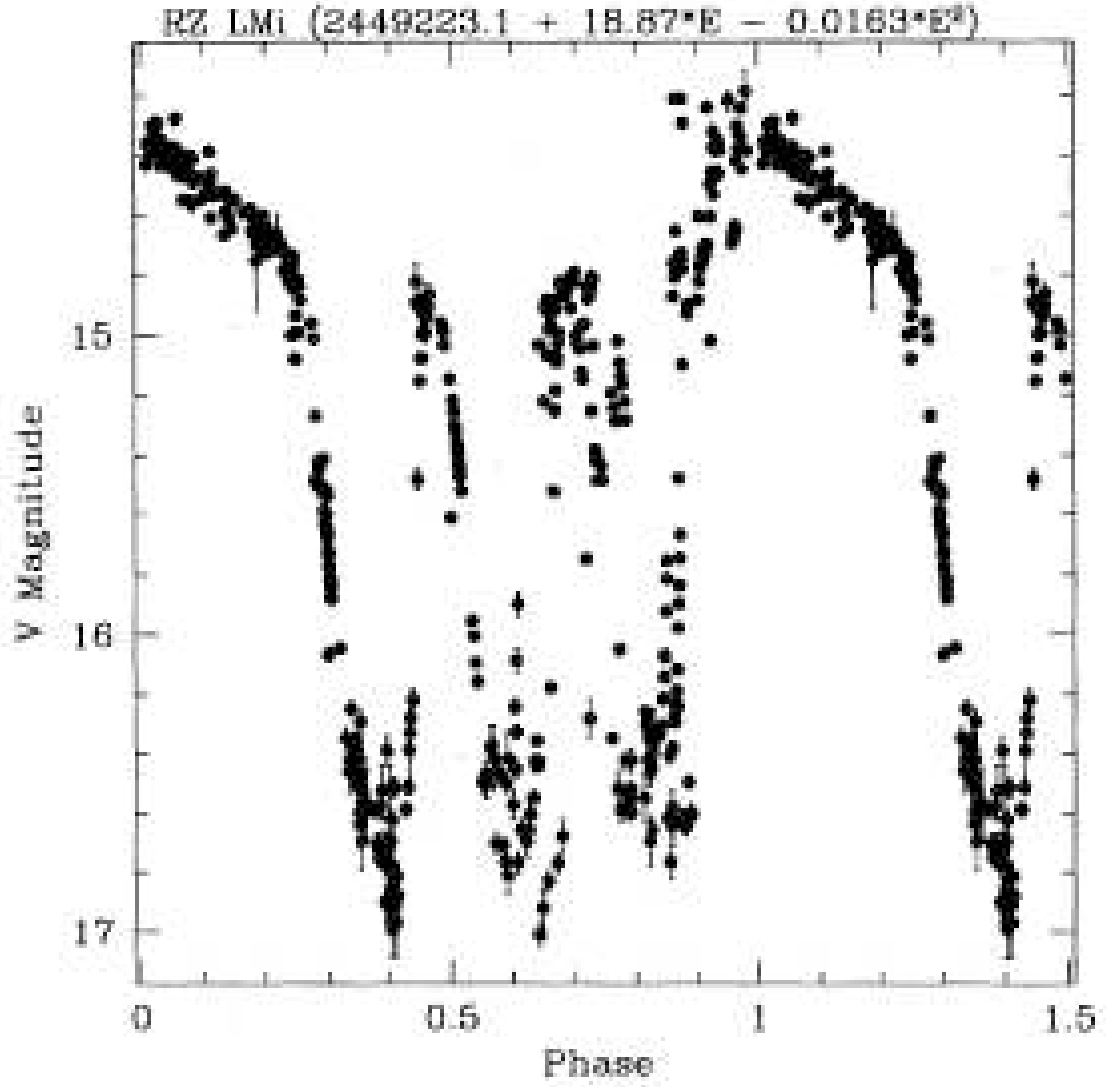
RZ LMi (2449223.1 + 18.87*E − 0.0163*E²)
V Magnitude
15
16
17
0
0.5
1
1.5
Phase

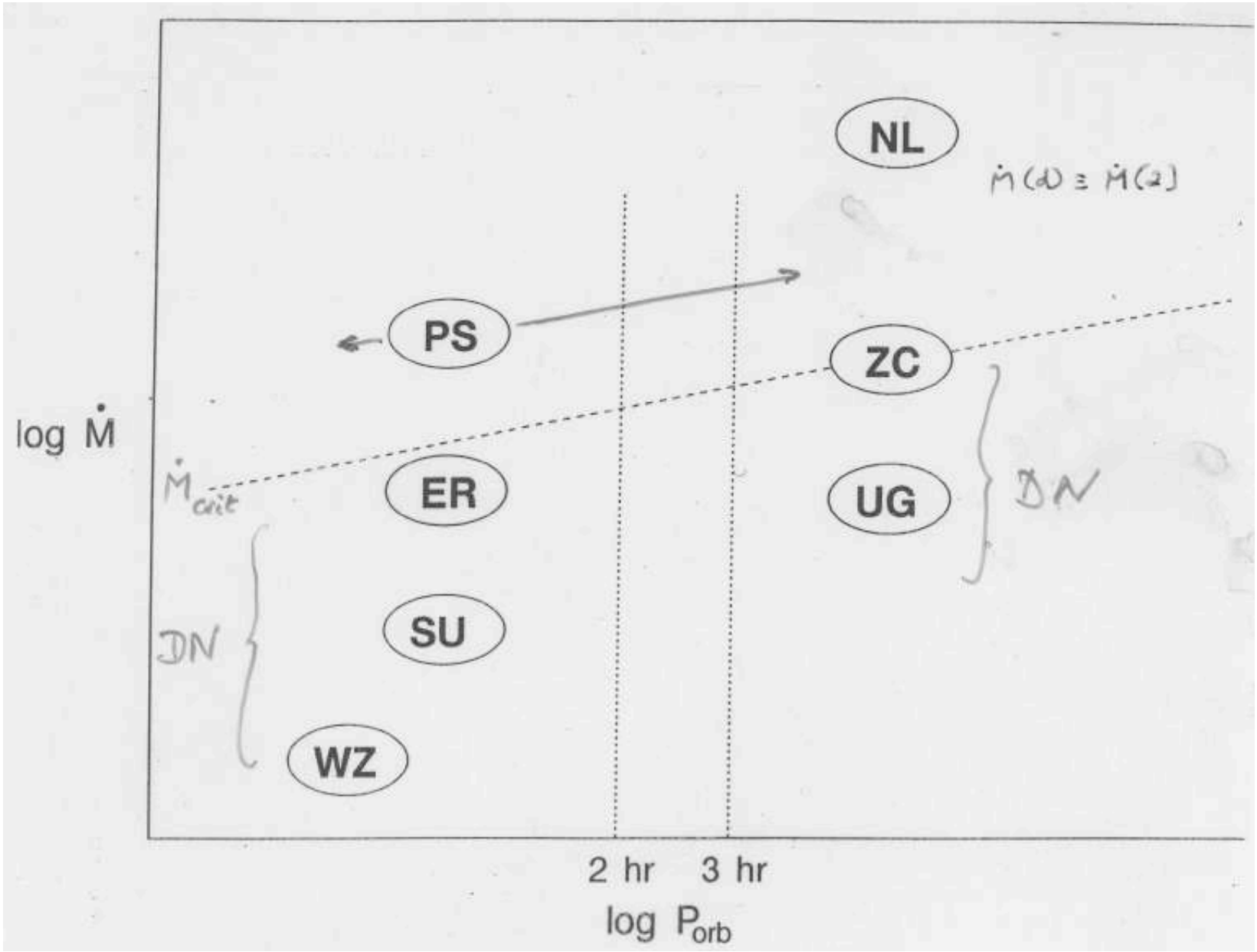
NL
$\dot{M}(d) \equiv \dot{M}(2)$
PS
ZC
log $\dot{M}$
$\dot{M}_{crit}$
ER
UG
DN
SU
DN
WZ
2 hr
3 hr
log $P_{orb}$

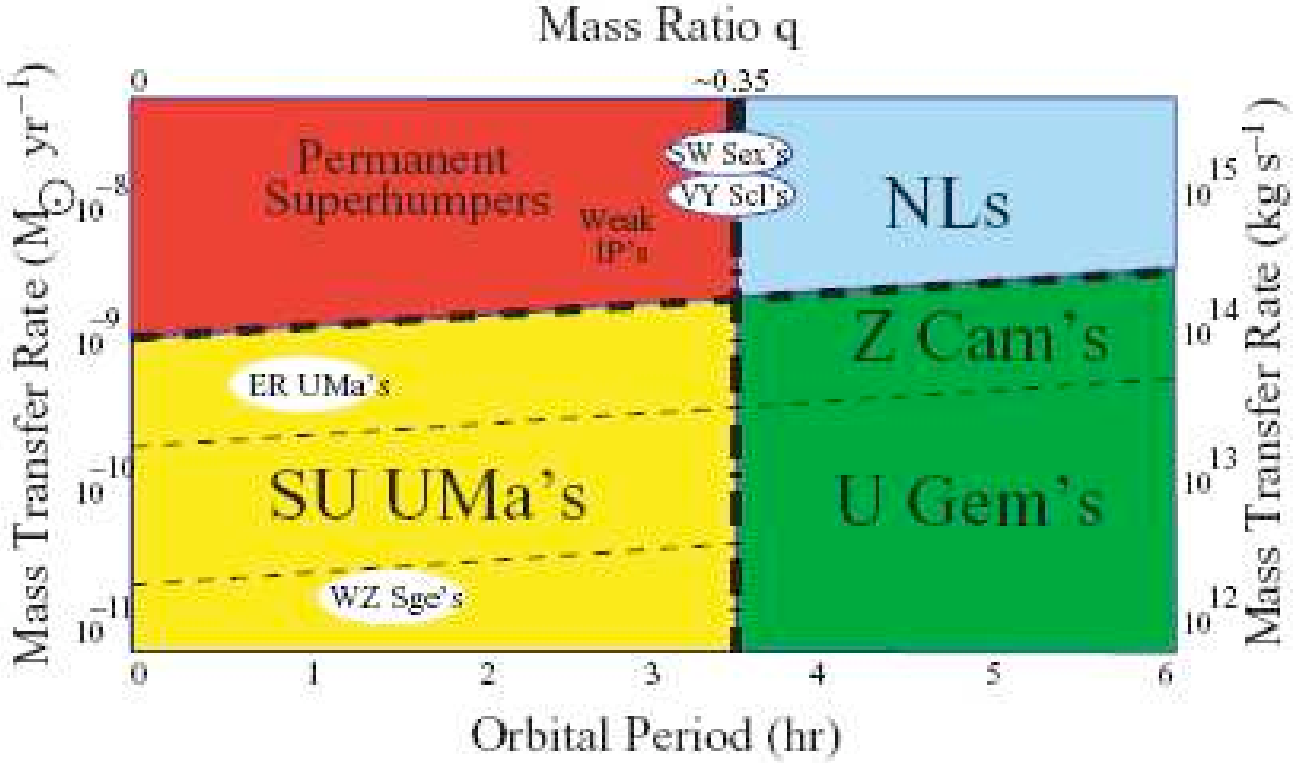
Mass Ratio q
0
~0.35
Permanent Superhumpers
SW Sex's
VY Scl's
Weak EP's
NLs
Z Cam's
ER UMa's
SU UMa's
U Gem's
WZ Sge's
Mass Transfer Rate ($M_\odot$ yr$^{-1}$)
$10^{-8}$
$10^{-9}$
$10^{-10}$
$10^{-11}$
Mass Transfer Rate (kg s$^{-1}$)
$10^{15}$
$10^{14}$
$10^{13}$
$10^{12}$
0
1
2
3
4
5
6
Orbital Period (hr)

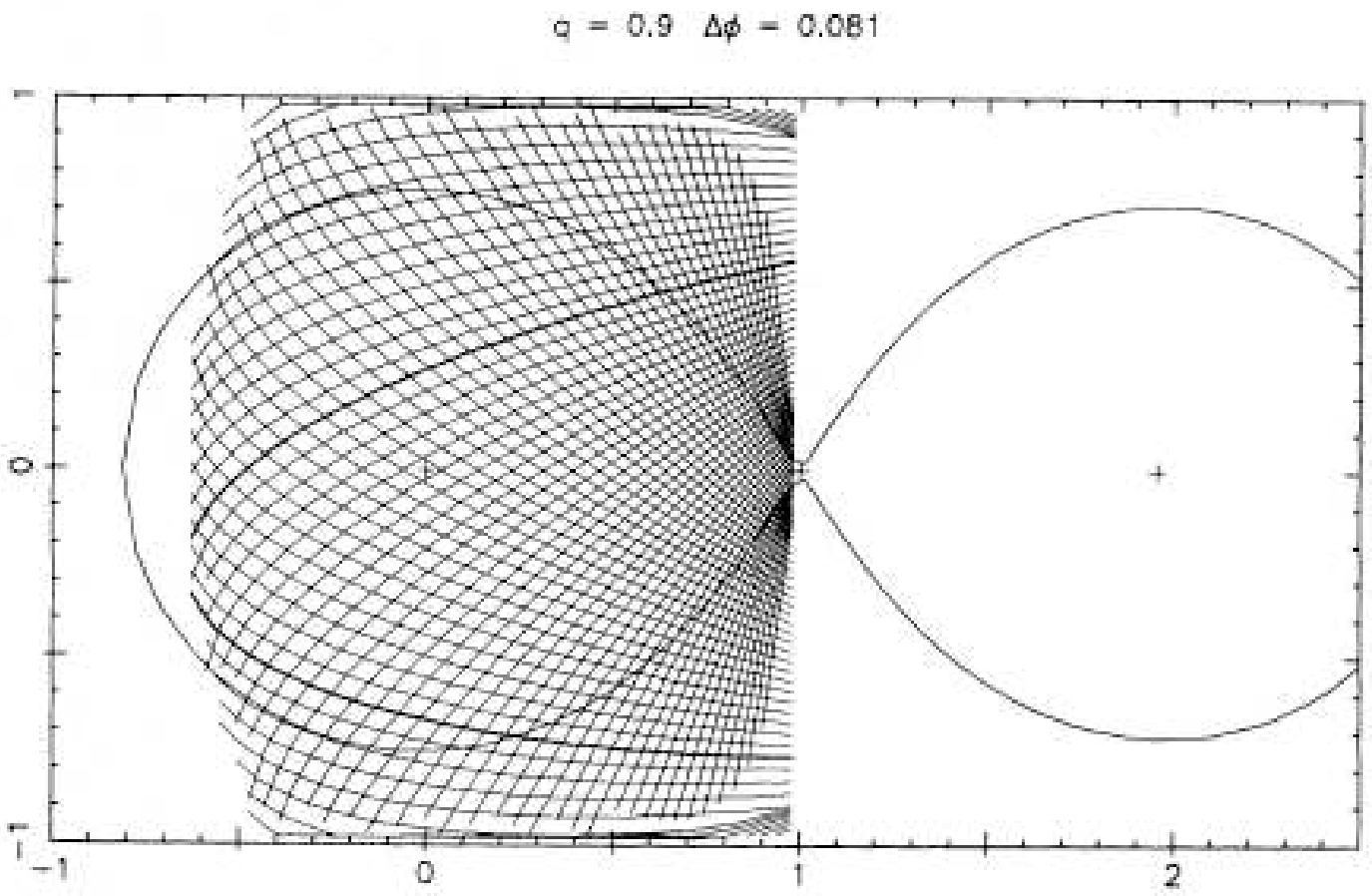


**Figure 3.** The geometry of an accretion disc eclipse is illustrated by a network of ingress/egress arches on the face of the disc. Each arch is the boundary of the disc region that is occulted by the red dwarf at a particular binary phase.

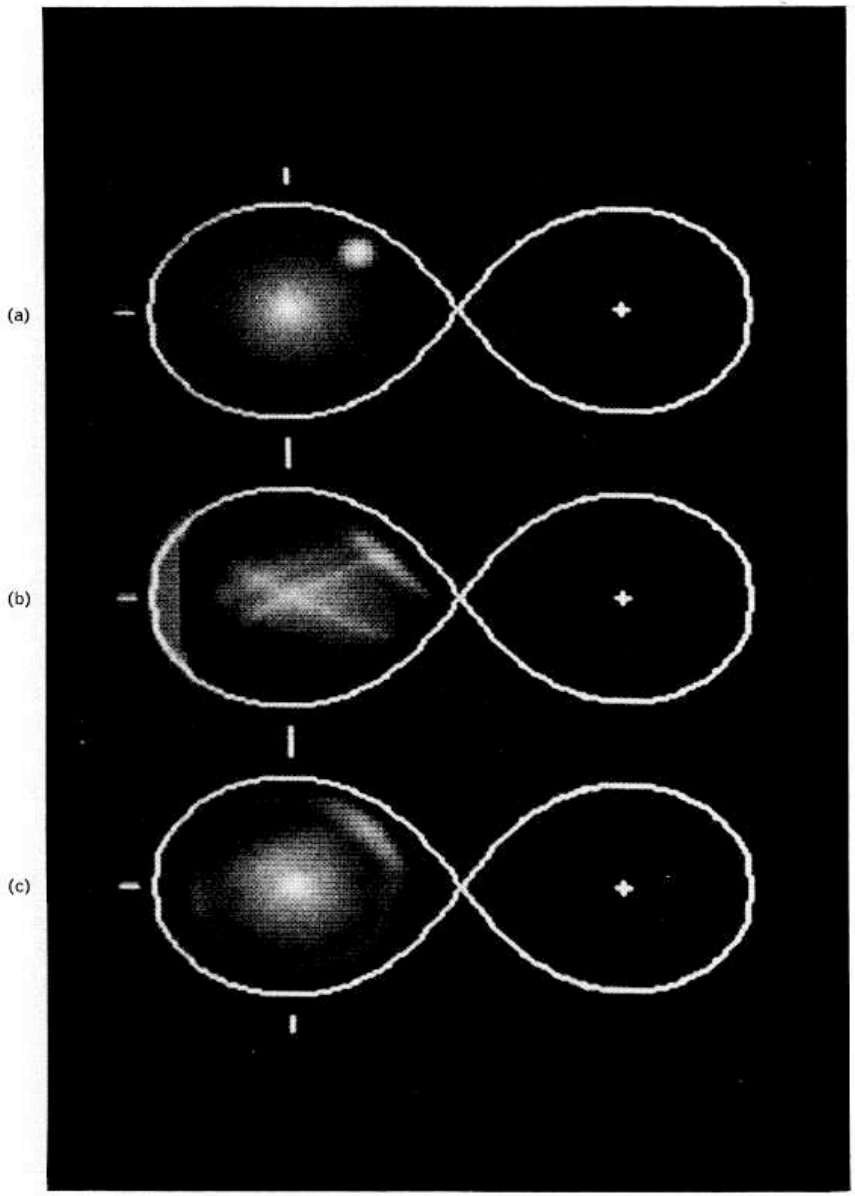


**Plate 1.** (a) This accretion disc image, the 5500 Å emission from a steady-state blackbody accretion disc with a Gaussian hot spot, was used to generate the light curve of Fig. 4. (b) The maximally uniform disc image reconstructed from the synthetic eclipse data of Fig. 4. (c) The maximally axisymmetric disc image reconstructed from the data of Fig 4.

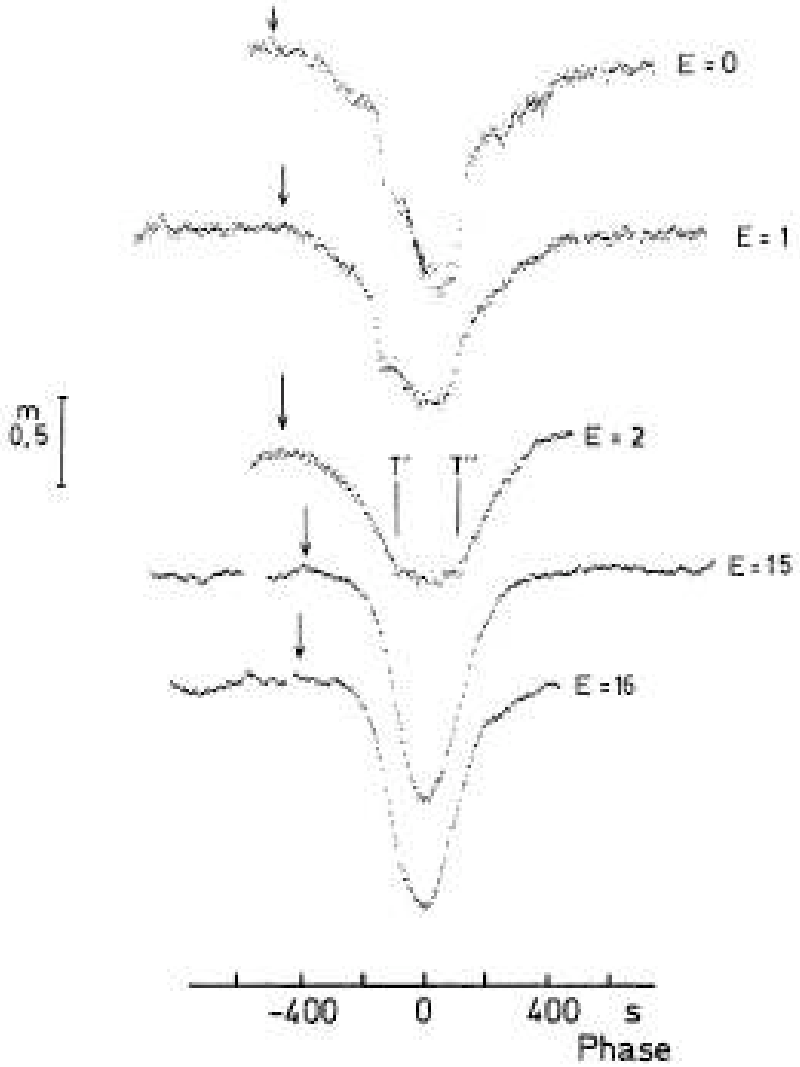


**Fig. 4.** Eclipse light curves of OY Car during rise ($E = 0, 1, 2$) and maximum ($E = 15, 16$) of the short eruption in April 1979. The phases refer to the ephemeris of Vogt et al. (1981). Arrows mark the ingress of the disc eclipse. Concerning significance of $T'$ and $T''$ see text

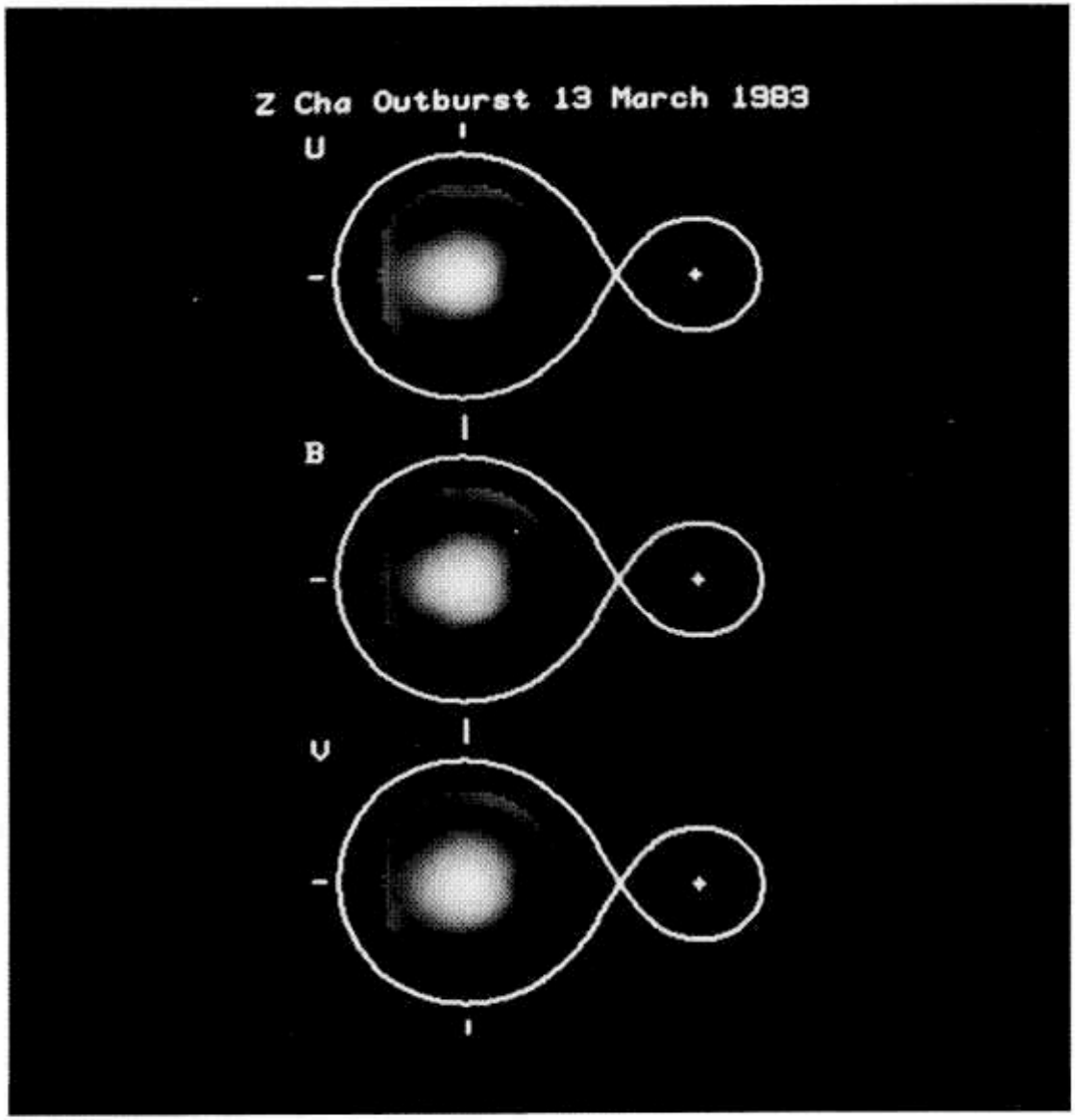


**Plate 1.** These accretion disc surface brightness distributions at $U$, $B$, and $V$ were reconstructed from the observed eclipse light curves. The light at all three wavelengths has a broad distribution that is concentrated toward the centre of the disc.

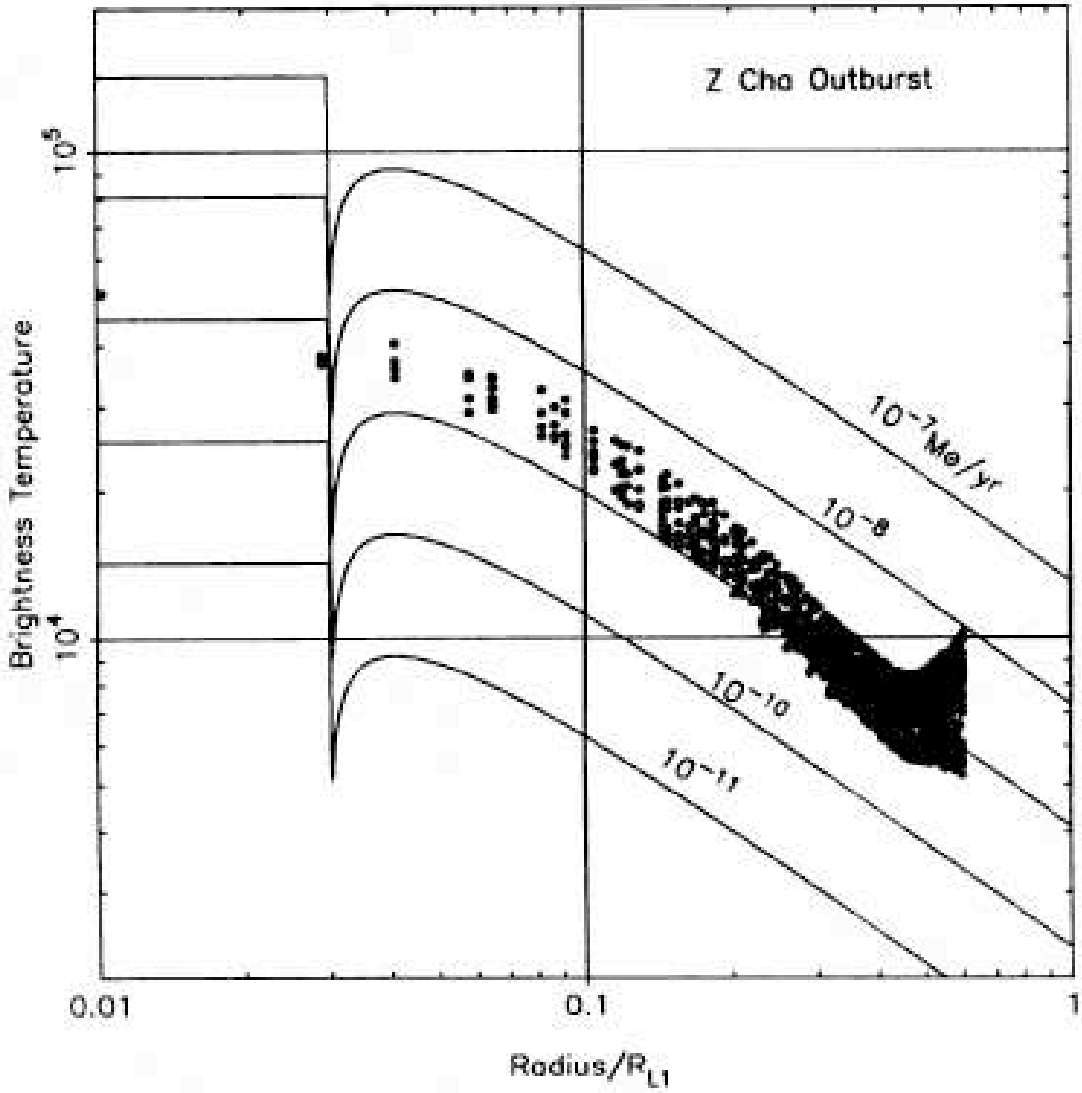


**Figure 6.** The observed temperature profile of the accretion disc is compared with the predicted temperature profiles of steady accretion discs at a range of accretion rates. Pixels with $R<0.03\,R_{L1}$ correspond to the white-dwarf surface, which has a temperature of ~40 000 K. The mass transfer rate in the disc is $10^{-9}\,M_\odot \mathrm{yr}^{-1}$.

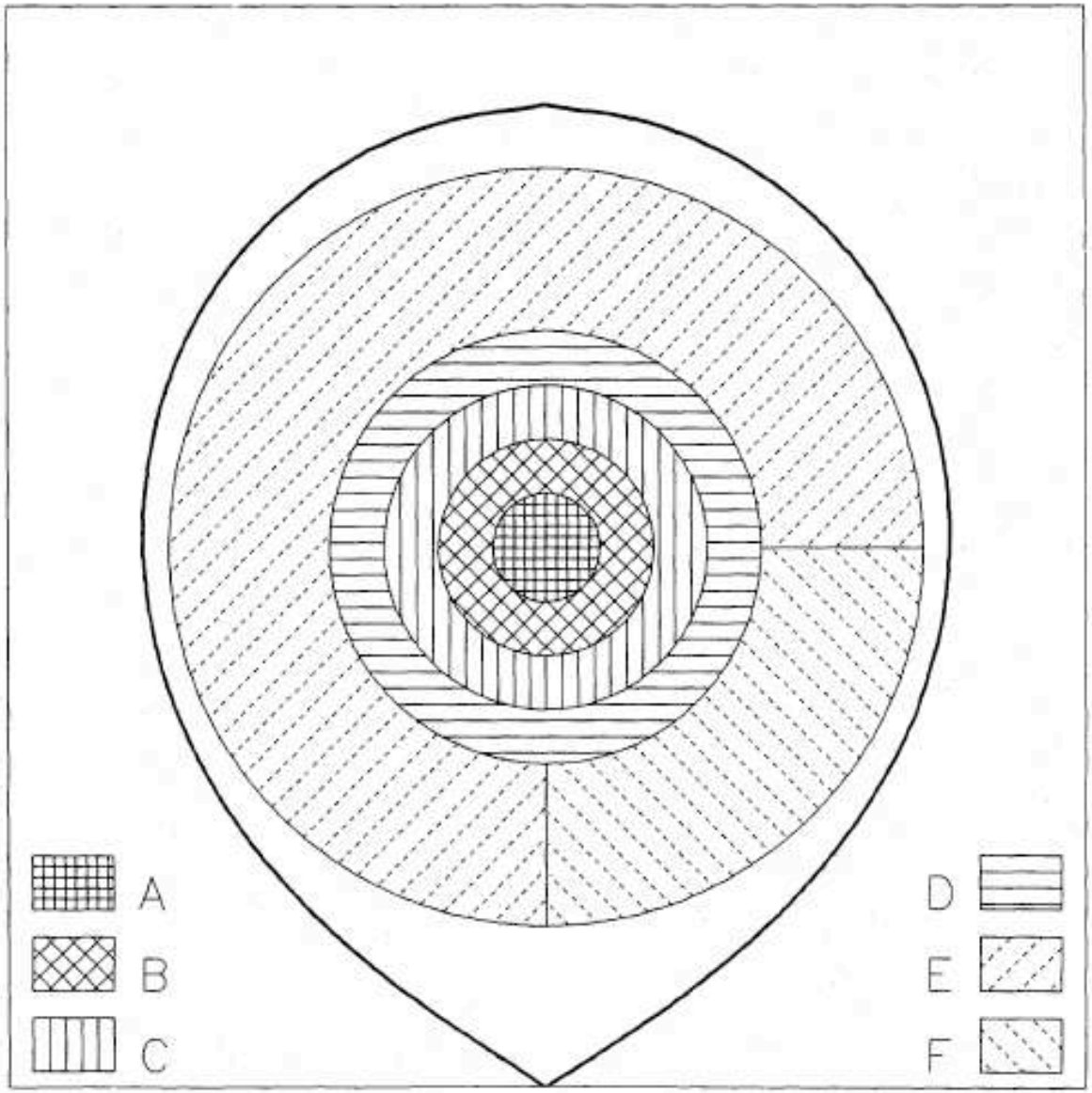


**Fig. 4.** Disk regions for which spectra are presented in Fig. 5 and Table 1. The bold line indicates the outline of the Roche lobe in the orbital plane

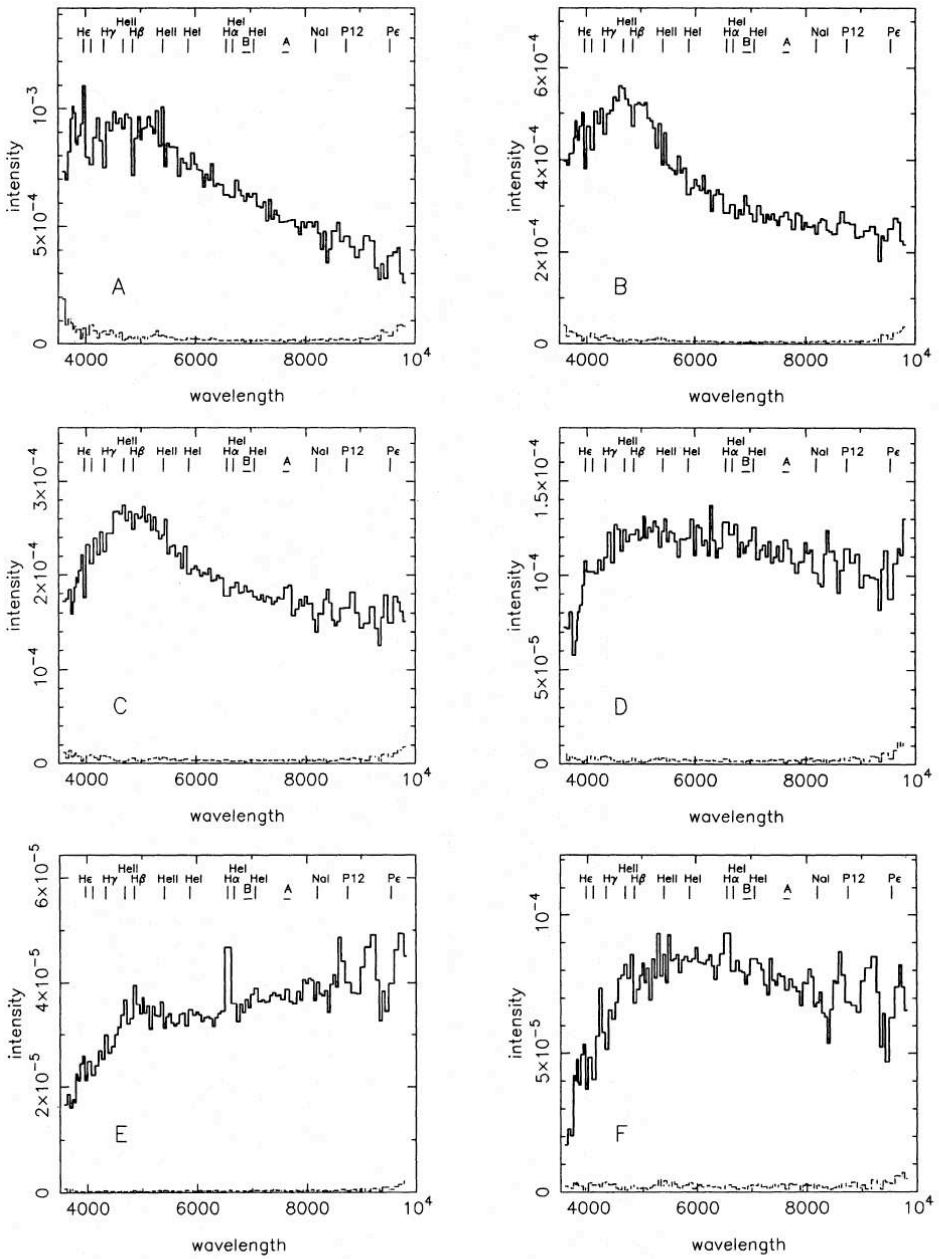


**Fig. 5a–f.** Specific intensities in erg cm$^{-2}$ s$^{-1}$ Hz$^{-1}$ ster$^{-1}$ as a function of wavelength for selected regions of the reconstructed accretion disk. The labels A to F correspond to the areas on the disk presented in Fig. 4. The dashed line shows the statistical uncertainty on each spectrum. The position of some of the main spectral features are indicated

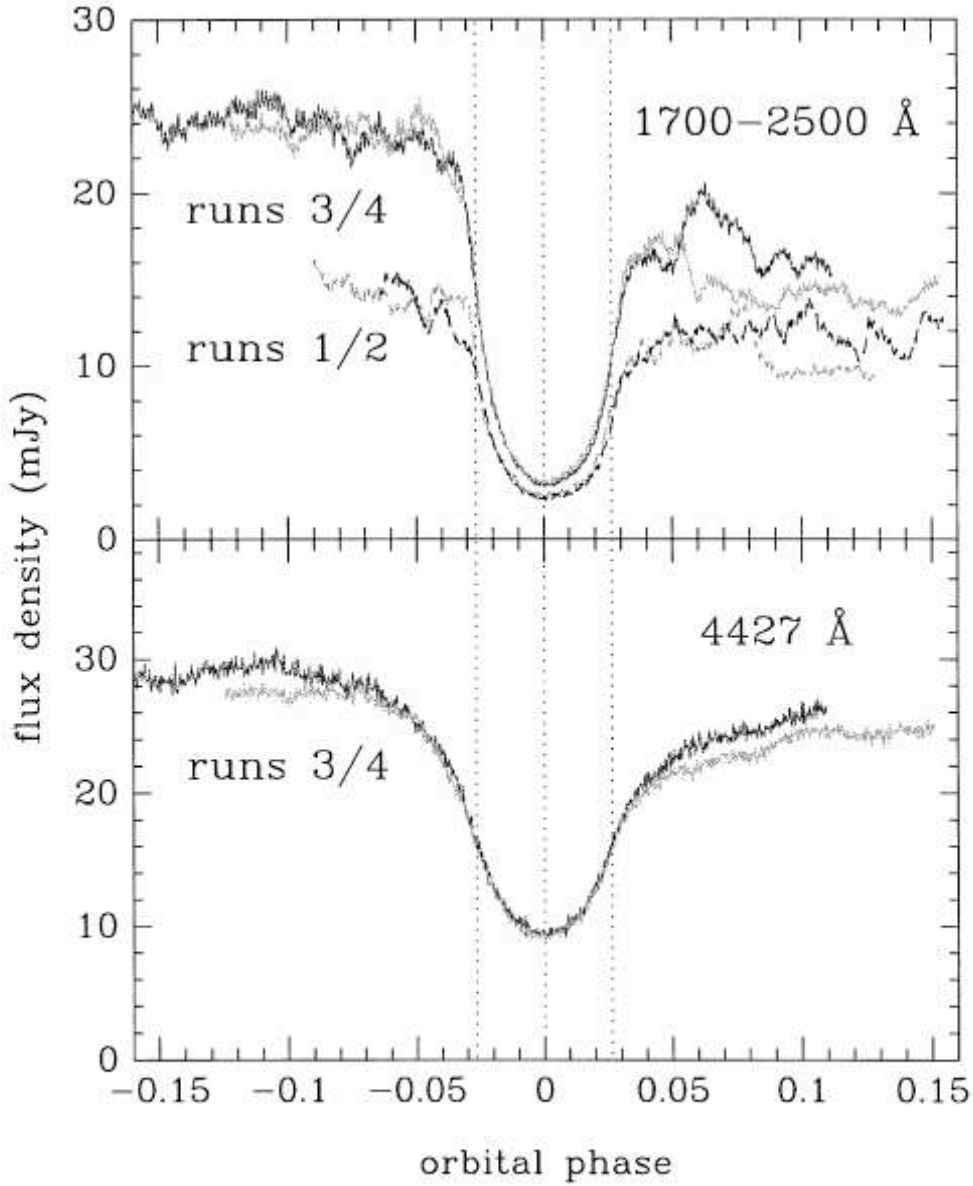


**Figure 1.** Top: light curves of the four *HST* runs at the same wavelength range. Bottom: light curves for runs 3 and 4 at λ4427. Vertical dotted lines mark ingress/egress phases of the white dwarf and mid-eclipse.

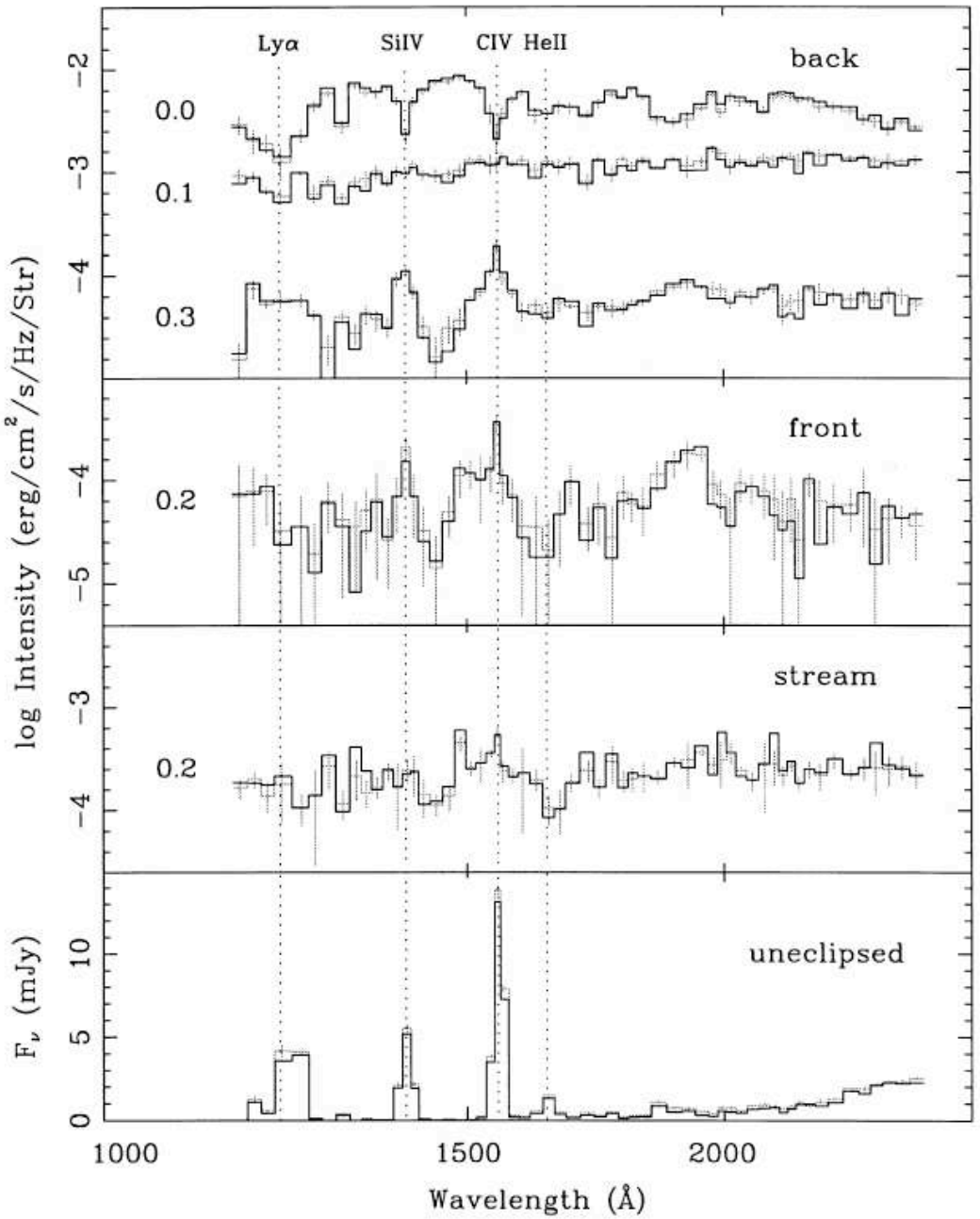
Lyα
SiIV
CIV
HeII
back
0.0
0.1
0.3
front
0.2
stream
0.2
uneclipsed
log Intensity (erg/cm²/s/Hz/Str)
F_ν (mJy)
Wavelength (Å)
1000
1500
2000

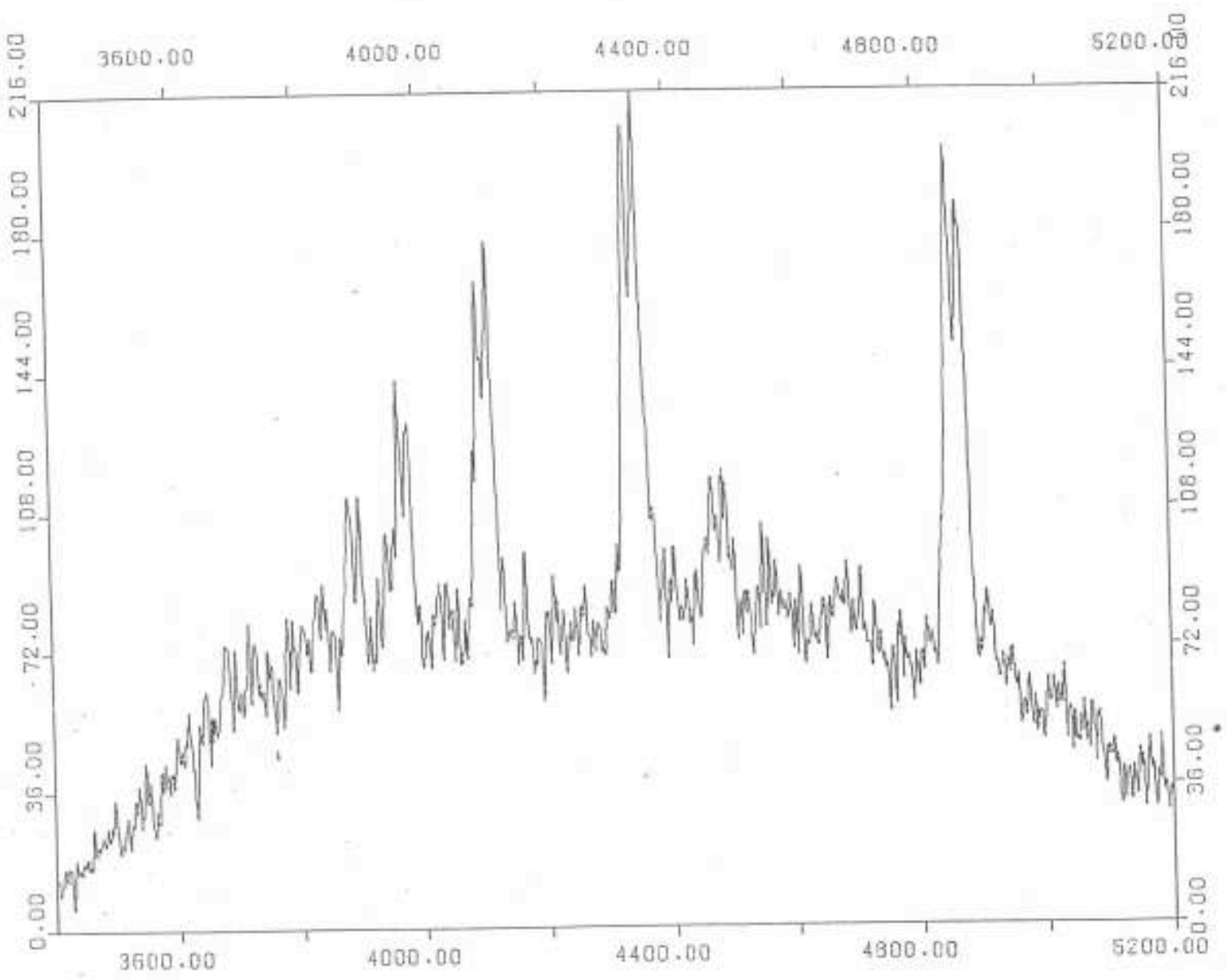
3600.00
4000.00
4400.00
4800.00
5200.00
216.00
180.00
144.00
108.00
72.00
36.00
0.00

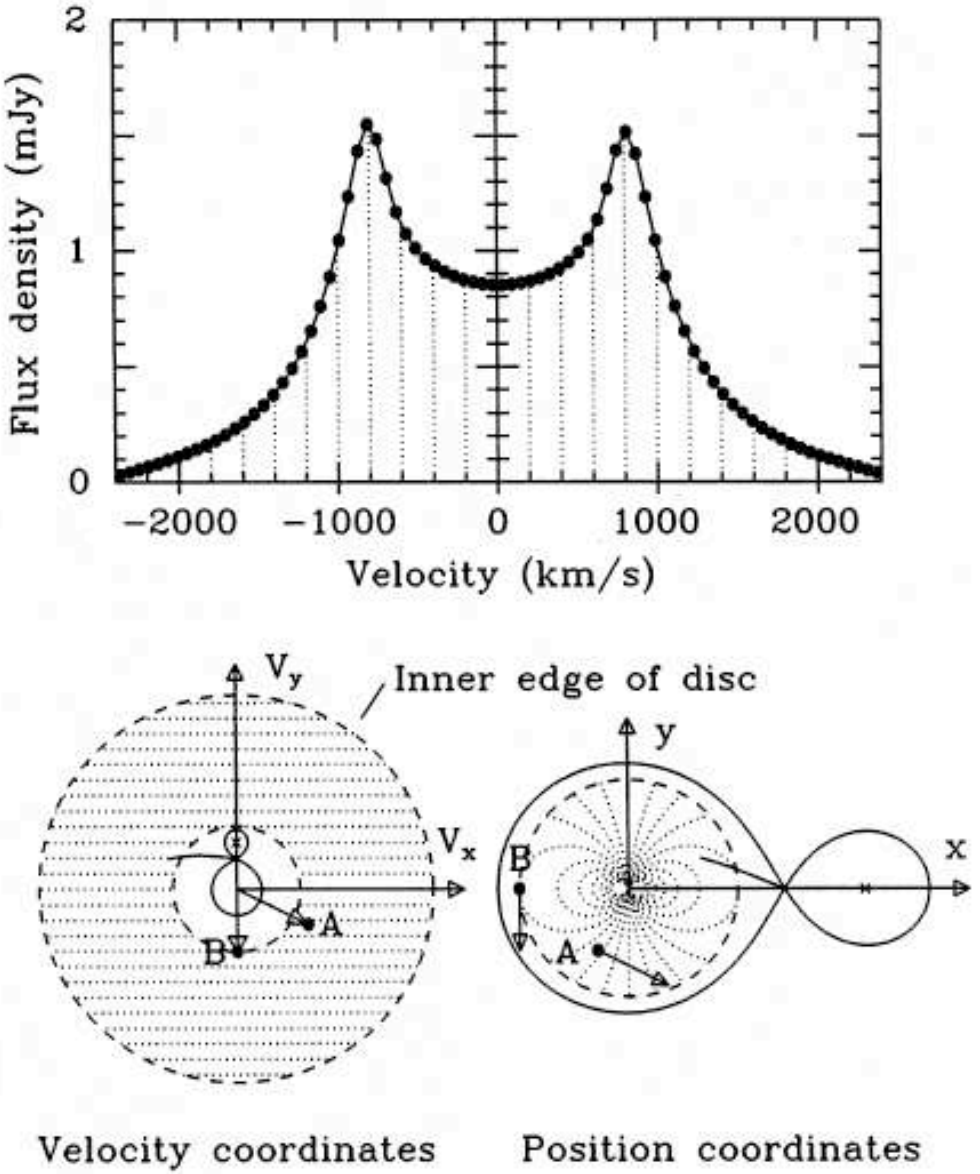


**Figure 1.** The lower right panel shows lines of equal radial velocity on an accretion disc for a disc in Keplerian rotation viewed at binary orbital phase 0.25 (observer looks from the bottom of the page). The upper panel shows the line profile that is formed from such a disc. Regions of equal radial velocity translate to the separate sections of the profile. The lower left panel is equivalent in velocity coordinates to the lower right. Lines of equal radial velocity are now straight but there are also equivalents in velocity coordinates for the red star and the gas stream. The points marked A and B in each picture are equivalent to one another.

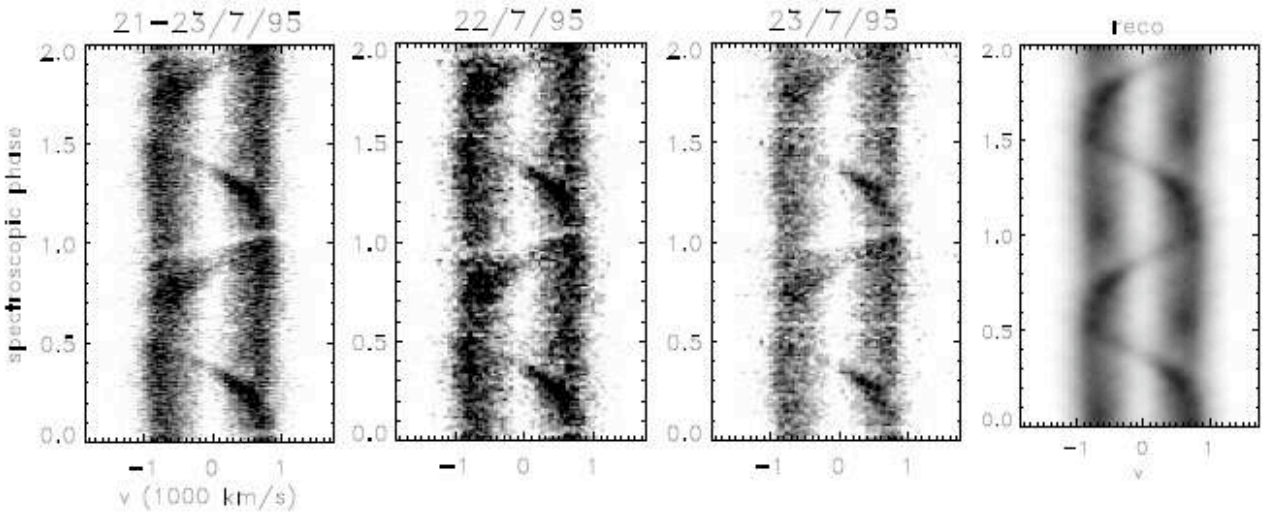


**Figure 1.** Hα spectra of WZ Sge. Left panel shows data covering about 12 orbits, obtained on three consecutive nights. Second and third panels show data from two of these nights separately. Phase is relative to inferior conjunction of secondary (see text). Note the absorption feature above the S wave at phases around 0.25–0.5. Right panel: reconstructed spectrum from the Doppler map of the leftmost panel.

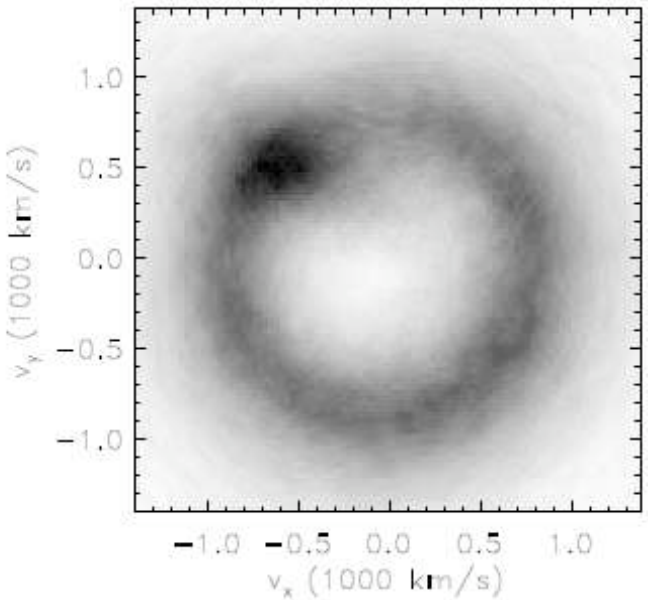


**Figure 2.** Doppler map from the leftmost spectrum of Fig. 1. Note absence of emission at the expected velocity ($v_x = 0, v_y = 600\,\mathrm{km\,s^{-1}}$) of the secondary.

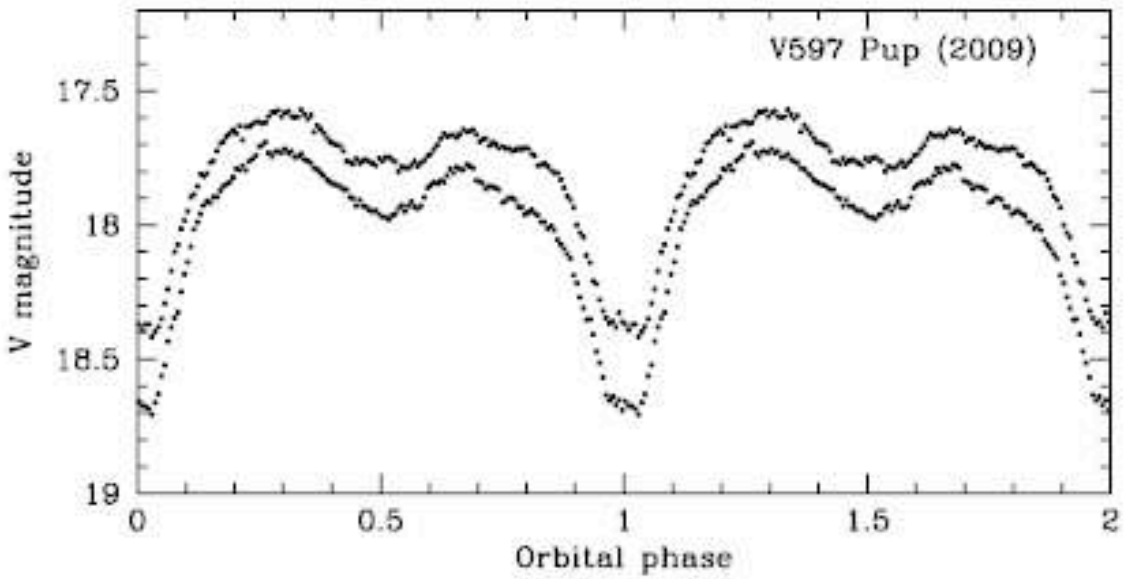


**Figure 5.** The average light curves of V597 Pup for the 2009 February and March observations, plotted separately.